Titanium nanoparticles fate in small-sized watersheds under different land-uses

Jia-Lan Wang, Enrica Alasonati, Paola Fisicaro, Marc F. Benedetti

Titanium nanoparticles fate in small-sized watersheds under different land-uses

Submitted to Journal of Hazardous material

Jia-Lan Wang[1, 2], Enrica Alasonati[2], Paola Fisicaro[2], Marc F. Benedetti[1]*

[1] Université de Paris, Institut de physique du globe de Paris, CNRS, UMR 7154, F-75238 Paris, France

[2] Department of Biomedical and Inorganic Chemistry, Laboratoire National de Métrologie et d'Essais (LNE), 1 rue Gaston Boissier, Paris, 75015 France

*Corresponding author
Email: benedetti@ipgp.fr (M. F. Benedetti)
Phone number: +33 1 83 95 76 95

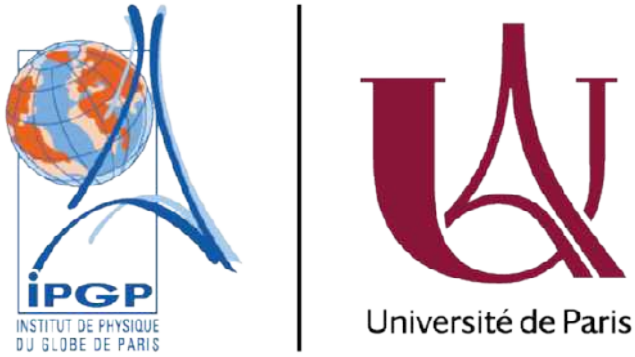

Highlights

The land-use has an impact on the TiO_2 nanoparticle concentrations, biogeochemistry, dynamics and exports rates.

- Higher amounts of small sized TiO_2 nanoparticles are detected by sp-ICPMS.
- Ti speciation varies with the type of soils and land-use.
- DOM controls the number of TiO_2 nanoparticles in surface water samples.
- Land-use impacts TiO_2 nanoparticles concentrations, dynamics and exports rates.

Graphical Abstract

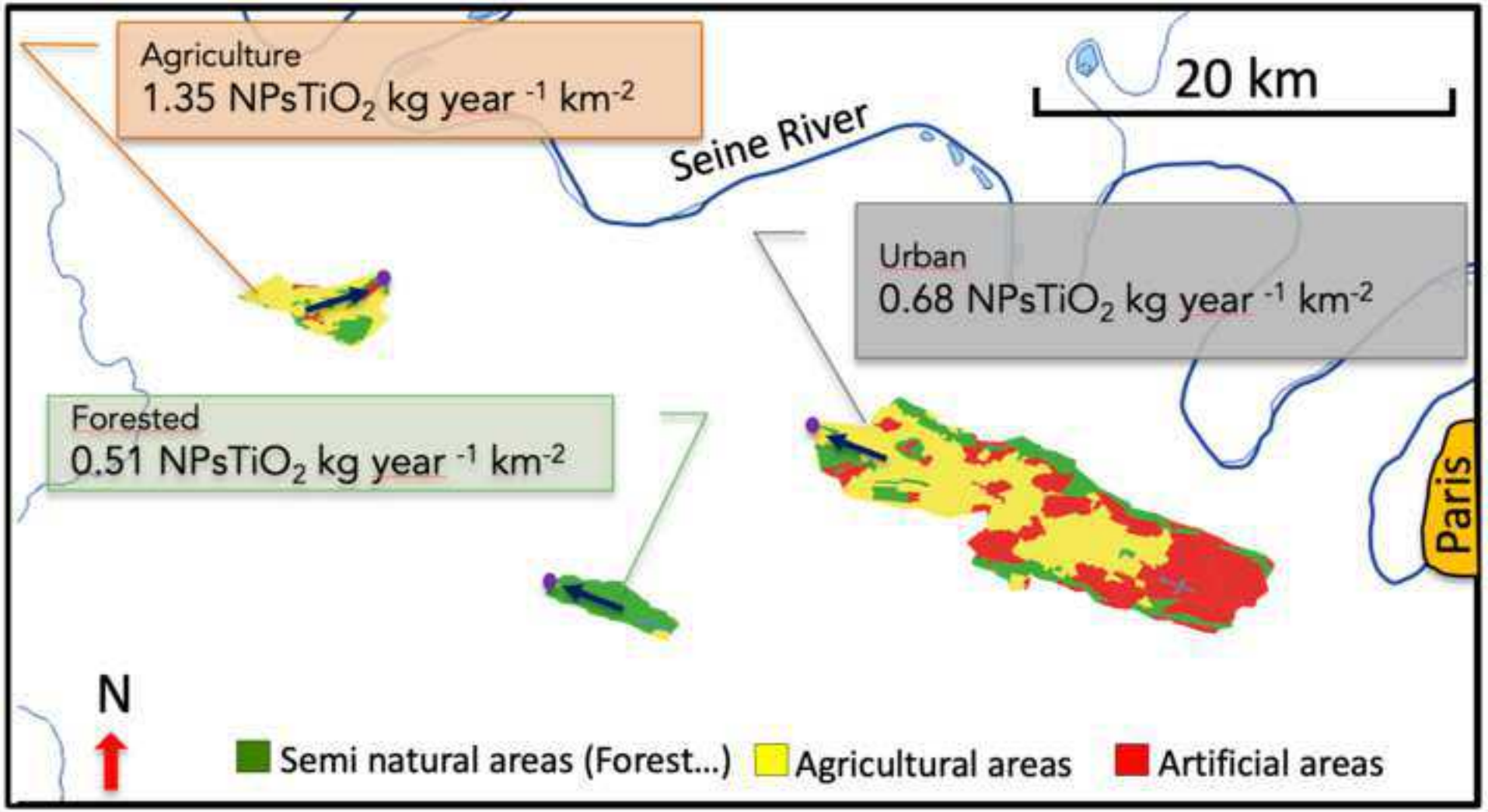

Titanium nanoparticles fate in small-sized watersheds under different land-uses

Submitted to Journal of Hazardous material

Abstract

Surface waters from three catchments having contrasting land-uses (forested, agricultural, and urban) were sampled monthly and analysed for nanoparticulate titanium dioxide (NPs-TiO_2) by single particle ICPMS and electron microscopy. We report one-year of data for NPs-TiO_2 having average number and mass concentrations of 9.1 x 10^8 NPs-TiO_2 particles L^{-1} and 11 µg NPs-TiO_2 L^{-1} respectively. An increase in concentration during warmer months is observed in the forested and agricultural catchments. Both concentrations of NPs-TiO_2 are within the range of recently reported values using similar analytical approaches. The positive correlations for NPs-TiO_2 mass concentration or particle number with the concentration of some trace elements and DOC in the forested and agricultural catchments suggest the detected NPs-TiO_2 in these two systems are mostly from geogenic origin. Additionally, microscopy imaging confirmed the presence of NPs in the three catchments. Furthermore, the land-area normalized annual flux of NPs-TiO_2 (1.65 kg TiO_2 $year^{-1}$ km^{-2}) was highest for the agricultural catchment, suggesting that agricultural practices have a different impact on the NPs-TiO_2 dynamics and exports than other land-uses (urban or forestry). A similar trend is also found by the reanalysis of recent literature data.

1. Introduction

Titanium dioxide (TiO_2) occurs naturally in rutile (TiO_2) and ilmenite ($FeTiO_3$) present in rocks and soils, with Ti annual cycling in the global surficial environment equalling up to 484 10^6

tons Ti y^{-1} [1]. Since early in the 20th century, particulate TiO_2 has been largely used as pigments in paints, papers and plastics because of its whiteness, high opacity and corrosion resistance. Owing to later milestone breakthroughs in TiO_2 research and the nanotechnology revolution, engineered nano-TiO_2 (en-TiO_2), defined as being < 100 nm in diameter, is more and more applied in other industrial uses [2]. Applications include foods, cosmetics, solar energy, and environmental remediation for instance. Engineered nano-TiO_2 has been reported as the most fabricated of all nanomaterial with 10^5 tons of en-TiO_2 used globally in 2015, and its production is predicted to increase at least by 2025 [3-4]. For France no such estimation of future annual use exists, but using the data from Switzerland [5] and extrapolating to France using its population as a scaling factor, an amount of 3,400 tons of en-TiO_2 y^{-1} is estimated for 2025 (i.e. 2,037 tons of Ti y^{-1}).

It is likely that en-TiO_2 will be discharged during or after its use into terrestrial and aquatic ecosystems, adding to the natural loads. For instance, in lab or land-scale studies, en-TiO_2 release into receiving waters has been reported from: exterior paints [6], textiles during washing [7], sunscreens [8], and construction and demolition landfills [9]. In addition, TiO_2 is a common food additive (known as E171 in Europe) and can be found in some dairy products, such as candies, chocolates, chewing gums, soups, nuts, milk and yogurt. A typical exposure of dietary TiO_2 for a US adult is estimated 0.2-0.7 mg TiO_2 $kg^{-1}$of body weight day^{-1} with most entering into wastewater treatment plants (WWTPs) [10]. Nanoparticle removal efficiency can be up to 96% [11-13] but the presence of en-TiO_2 in effluents after treatment is still identified at the level of µg L^{-1} [13]. These studies demonstrate that en-TiO_2 has entered our aquatic systems and therefore evaluating the potential risk to ecosystems, as well as to humans, through bioaccumulation is of great importance.

Manufactured TiO_2 is not the only source of Ti in the environment. It is estimated that 375 x 10^9 kg of Ti per year are displaced by soil erosion at the world scale [1]. Fifty percent of this flux was of anthropogenic origin mostly because of the influence of agricultural practices on erosion fluxes [1]. The GEMAS project reported the concentration of Ti in agricultural soils for Northern Europe to be equal to 3.11 g of Ti kg^{-1}, accounting for the high erosion flux value resulting from agricultural practices [14]. In addition, the flux of Ti due to coal burning was estimated at 4.9 x 10^9 kg of Ti per year using a concentration of 0.8 mg Ti kg^{-1} coal [1]. The other major global source of Ti flux are construction activities that correspond to a flux of 43 x 10^9 kg of Ti per year [1]. All those fluxes are several orders of magnitude higher than an annual global en-TiO_2 flux equal to 409 x 10^6 kg per year based on Europe's estimation [4] and extrapolated to the world using world population as a scaling factor. This complex global and local biogeochemical Ti cycle complicates the understanding of the respective fate of en-TiO_2 vs natural and/or other anthropogenic sources of nanoparticulate TiO_2 in the critical zone [15]. The sum of the three potential types of nanoparticulate TiO_2 is defined in this paper as NP-TiO_2 = en-TiO_2 + natural Ti + other anthropogenic Ti sources.

To investigate NP-TiO_2 fate and ecotoxicity in aquatic systems, quantitative measurement is a primary step. However, it is a challenging issue because of low predicted concentrations and high Ti background [16] and the analytical limitations for nanomaterials [17]. Although the exposure of various types of en-TiO_2 has been modelled based on their production volumes and their foreseen pathways, these predictions must be validated by "real world" data [18]. There is a consensus that the lack of field data is always the key knowledge gap [19]. Few relevant studies have been conducted at the field scale to detect nanoparticles (NPs) like

Nano-Ag, TiO_2, CeO_2 or carbon nanotubes [8,20-26]. These field measurements begin to allow construction of an NP-TiO_2 database, which helps to better understand both their fate in the environment and to conduct ecological risk assessments.

Few studies have investigated the temporal changes in NP-TiO_2 concentrations arising due to hydrological and meteorological variability along the year. Moreover, most field measurements in freshwater were done at one or several sites but along the same river, focusing mostly on the characterization of Ti-containing nano - or colloidal particles. The identification of processes and drivers potentially controlling the fate of NPs is still lacking at the field-scale. Additionally, natural contribution to environmental concentration, in the case of TiO_2, makes all abovementioned research more challenging. It is therefore complicated to understand the variations in concentrations, not to mention identifying the possible drivers of those changes against a high geochemical background [14-15]. However, recently the contribution of en-TiO_2 in sewage spills to impacted surface waters was identified and quantified with single particle counting TOF-ICPMS (Time Of Flight Inductively Coupled Mass Spectrometry). Concentration of en-TiO_2 up to 95 µg L^{-1} were reported [24] which is a very high value compared to predicted values [4].

Little is known about watershed scale processes regarding NP transport. With the data from Peters et al.,[22] we calculated the mean annual mass of NPs-TiO_2, leaving the Ijssel and Meuse watersheds and the export rate normalized to the watershed area (in kg NPs-TiO_2 $km^{-2}y^{-1}$). The average annual discharge rate and watershed area for the Ijssel and the Meuse are 390 m^3sec^{-1}, 357 m^3sec^{-1} and 4,270 km^2, 36,000 km^2, respectively [27-29]. For the Ijssel and the Meuse rivers, the calculated flux annual, normalized export-rate are equal to 45.5 t NPs-

TiO_2 y^{-1}, 10.9 kg NPs-TiO_2 km^{-2} y^{-1} and 26.9 t NPs-TiO_2 y^{-1}, 0.8 kg NPs-TiO_2 km^{-2} y^{-1}, respectively. The very different NPs-TiO_2 normalized export-rate values obtained for both rivers suggest that different processes or sources regulate the concentrations of NPs-TiO_2 in those two watersheds.

It is hard to identify sources and/or processes regulating NP-TiO_2 concentrations by performing measurements at a single or even multiple points along a river without taking into account land-use and the annual hydrological variability and their geochemical implications. Field sites under different land-uses, from less-impacted environments to catchments heavily impacted by urban activities, need to be investigated for a better understanding of NP-TiO_2 dynamics. The present study had 3 mains objectives: 1st to collect 1 year of NP-TiO_2 measurements in three catchments with variable geochemical characteristics and diverse land-uses to monitor the relevant concentration of NP-TiO_2 in freshwaters; 2nd to assess the potential processes controlling NP-TiO_2 in natural waters from small watersheds with variable local weather, hydrology and anthropogenic activities and 3rd to address the impact of land-use, at the scale of small size sub-basins, on the export-rates of NPs-TiO_2 and total Ti from the catchment. Given that NP-TiO_2 have been suggested to serve as a tracer of other engineered nanomaterials [11], these investigations could be useful for evaluate the general transport and fate of widely used engineered nanoparticles in aquatic systems.

2. Materials and Methods

2.1 Sampling and analysis

2.1.1 Sampling sites

Stream waters were sampled from three sub-basins in the Seine River watershed located in the West of Paris, France (Fig. 1). The Seine River watershed has a total area of about 67,500 km^2 and is located in a sedimentary basin [29]. Sampling of smaller sized sub-basins is justified because they are prone to react more quickly to hydrological, meteorological and anthropogenic effects. The three selected watersheds had been used in previous studies on the origin and dynamics of trace metals and silver nanoparticles [25,30-31]. They have different lithologies (i.e. sandy vs carbonate) and land-uses, namely forested, agricultural and artificial surfaces. Their characteristics are detailed in Fig. 1 and Table S1. The urban watershed is a good analogue of the larger Seine river watershed as it is a representative mixture of the overall Seine watershed land-uses (i.e. the ratio of artificial areas vs agricultural areas) [25,30-31].

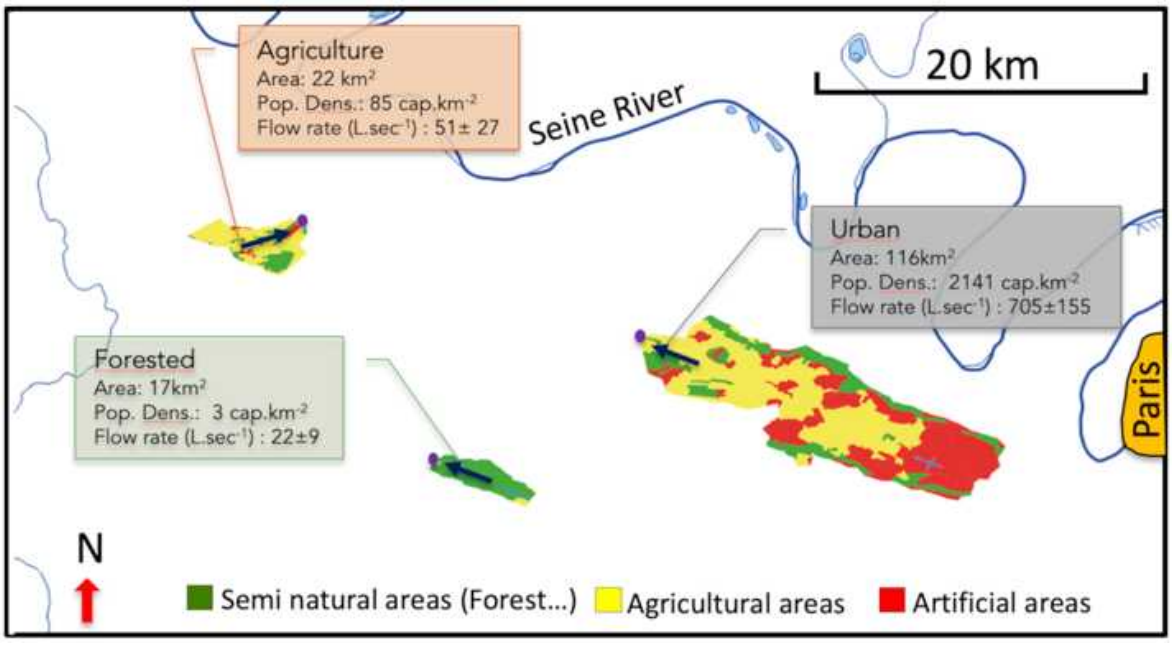

Fig. 1: Sampling location and their land-use. Blue arrows indicate the direction of the water flow. Coloured boxes report the area of the watershed, the average population density (Pop. Dens.) and measured annual average water flow rate ($L.sec^{-1}$) for each watershed.

136

137 2.1.2 Sample collection and analysis

138 Water samples were collected once per month from November 2016 to December 2017. Grab
139 surface water samples were collected in 1 L HDPE bottles pre acid-washed (HCl 1N for 2 days)
140 and rinsed in ultrahigh purity water (Milli Q water). Various physicochemical parameters were
141 monitored to comprehensively characterize the aquatic geochemistry. They include pH,
142 dissolved oxygen, conductivity, alkalinity, dissolved organic carbon (DOC), major anions,
143 cations, trace elements and rare earth elements (REEs). The detailed analytical protocols and
144 data can be found elsewhere [25]. In the laboratory, 500 mL of each bulk water sample used
145 for nanoparticle analysis was ultra-filtered through a 1 kDa regenerated cellulose membrane,
146 which corresponds to about 1.3 nm in membrane pore size [32], in order to remove all the
147 particles smaller than a few nanometres. This ultra-filtrate was further used as the matrix to
148 prepare all standards and solutions for single particle ICPMS analysis.

149

150 2.1.3 Bulk water chemical analysis

151 The total concentrations of Ti, Ni, Cu, Zn, As, Sb, Cd, Pb in bulk water samples were determined
152 by ICPMS after complete acid digestion. A mixture of 3 mL HCl, 1 mL HNO_3 and 0.5 mL HF (ACS
153 grade acids distilled in the laboratory) was added to 10 mL of raw water into a 30 mL PFA
154 Savillex digestion vessel. The well-closed Savillex vessel was heated at 105 °C during 24 hours.
155 After digestion, the mixture was evaporated at 85 °C to dryness. The residue was then re-
156 dissolved in 10 mL of 2% HNO_3. The blank of the digestion procedure was evaluated with ultra-
157 pure water by following the same procedure. Each sample digestion was performed in
158 triplicate. The protocol was validated by digestion of commercial standards of TiO_2

159 nanoparticles (P25 and AERODISP-W740-X) at concentrations ranging from 20 µg L^{-1} to 400
160 mg L^{-1}. Satisfactory recovery factors above 90% were obtained (Table S2).
161
162 2.2 Quantification of TiO_2 NPs by single particle ICPMS (sp-ICPMS)
163 2.2.1 Instrumental operating parameters
164 A sector-field ICPMS (Element II, Thermo Scientific) was used for sp-ICPMS measurement of
165 NPs-TiO_2. Before sample analysis, the ICPMS instrument was first tuned to ensure a good
166 sensitivity, stability and low oxide formation. The instrument was operated in medium
167 resolution mode, which provides sufficient resolution (> 4,000) to avoid isobaric or
168 polyatomic interferences on ^{48}Ti. The operating conditions are detailed in Table 1. The sample
169 uptake flow was determined by weighing the sample before and after a fixed period (i.e. 15
170 minutes), then dividing the mass difference by time. These measurements were systematically
171 performed at the beginning, middle and end of analysis sequence.
172
173 Table 1: Experimental conditions of sp-ICPMS measurement.
174

Parameter	**Experimental conditions**
Spray chamber	Quartz cyclonic
Nebulizer	PFA MicroFlow
Plasma power	1315 W
Cool Gas	16 L min^{-1}
Auxiliary Gas	1 L min^{-1}

Peristaltic pump rate	12 rpm
Uptake flow	≈ 0.2 mL min^{-1}
Monitored isotope & resolution	Low Resolution: ^{197}Au Medium Resolution:^{47}Ti
Dwell time	1 ms
Settling time	1 ms
Data number	10,000

175

176 2.2.2 Standard and sample preparation

177 A suspension of 60 nm gold nanoparticles (NIST, RM8013) was used to determine the
178 transport efficiency. The working standard was freshly prepared by diluting the stock
179 suspension to about 200 ng L^{-1} with the ultra-filtrate of stream waters. Ionic calibration
180 standards (Au: 50 to 5000 ng L^{-1}; Ti: 0.2 to 10 µg L^{-1}) were prepared to determine element
181 sensitivity (dissolved or particulate form) by diluting the stock standards at 1000 mg L^{-1} in the
182 ultra-filtered matrix. Transport efficiency was calculated for each sampling mission and the
183 value was equal to 9% ± 2% [25].
184 The dilution of raw waters was usually performed to reach the proper number of particles for
185 accurate sp-ICPMS measurements. Here, dilution by 10, 50, 100, 500 times were tested, with
186 the best dilution factor varying from one sampling collection date and/or sampling site to
187 another. During each analysis the raw waters were diluted with the ultra-filtered matrix (i.e.
188 fraction of the water < 1 kDa, as previously described) and dilutions were performed until the
189 size distribution of the NPs-TiO_2 did not change. The samples were not sonicated prior to

190 measurements to be as close as possible to the field conditions. All standards and samples
191 were prepared daily, with the minimum delay until sp-ICPMS measurements.
192
193 2.2.3 Data analysis
194 Theoretical descriptions and calculations of sp-ICPMS are well established in literature [33-39].
195 The data analysis in this study is mainly based on procedure described by Pace [39]. The only
196 difference is that a different method called “subtraction method”, extensively described
197 elsewhere [25], is applied here to distinguish NPs from the background. The method is
198 summarized in the supplementary material section 1 and [25].
199 The annual average enrichment factor (EF) is calculated by a double normalization of the
200 average annual total element concentration ([Me]) in the sample ([Me]/[Y])sample) to the
201 same element ratio in a reference sample (([Me]/[Y])reference),
202
203 EF[Me] = ([Me]/[Y])sample/([Me]/[Y])reference
204
205 Yttrium was chosen as the reference element since the usual reference elements (Th, Al) were
206 not measured. In addition, Yttrium has no known biological role that would prevent it use as
207 a reference element.
208
209 2.2.4 Evaluation of the uncertainty on nanoparticles’ number
210 According to the Guide to the expression of Uncertainty in Measurement (GUM), the standard
211 uncertainty of measurand can be obtained by propagating the variances of the related
212 parameters [40]. Several factors are identified as contributors to the uncertainty in case of sp-
213 ICPMS measurements of nanoparticles in natural waters such as the solution preparation,

calibration, sensitivity of ICPMS, field sampling and sample stability. Two main contributions are taken into account in this paper i.e., the measurement repeatability (u1) and the sampling variability effect (u2), for the concentration of nanoparticles determined by sp-ICPMS. The calculation procedure is developed in the supplementary section and an example of calculation is given in Fig S5.

2.3 Electron Microscopy observations

A Carl Zeiss Auriga Field Emission Gun – Scanning Electron Microscope (FEG-SEM) was used to image Ti-bearing particles. It is equipped with secondary and backscattered detectors for the morphology and contrast in chemical composition of analysed particles. The FEG-SEM analysis was performed at electron energy of 5 to 15 keV. The coupled energy dispersive X-ray spectroscopy (EDX) provided elemental compositions of detected particles. The microscopy analysis was performed randomly on two out of ten samples (i.e. 25/09/17 and 19/12/17)) to confirm the presence of NPs-TiO_2 detected by sp-ICPMS and to gain qualitative knowledge on their shapes and sizes. The fresh raw waters were first filtered through 0.45 µm (Polycarbonate) and a 0.2 µm (acetate cellulose) and then a 1 kDa polyether sulfone filters. These filtration steps were meant to collect the particles on the filters and subsequently observe the particles on the filters. The filters were air-dried overnight in a clean room. The dried filters were then cut into 1 cm per 1 cm squares and coated with gold. Each filtration of raw water was performed in triplicate together with one blank of ultrapure water.

3. Results and Discussion

3.1 Physicochemical characteristics of three catchment waters

238 The three watersheds, where freshwater samples were taken, have different percentages of
239 three land-uses (i.e., forested, agricultural and artificial; Table S1) and are thus impacted by
240 natural processes or anthropogenic activities to different degrees. Our previous studies on the
241 same sites demonstrated that they differ in terms of geochemical background and heavy
242 metal sources (ex. Zn dynamics) or silver NPs (Ag-NPs) dynamics [31,25]. Number and mass
243 concentration of NPs-TiO_2 derived from these watersheds should vary along the year and
244 differ among sites. In addition, the fate and the behaviour of NPs-TiO_2 should be influenced
245 by matrix properties, such as pH, ions (identity and concentration) and dissolved organic
246 matter (i.e. DOC). The properties of catchment's water are summarized in Table 2 according
247 to previously published data [25]. The water of the forested catchment has a near-neutral pH
248 and the lowest ionic strength (as represented by conductivity), but higher DOC concentrations
249 due to the sandy nature of the soils (Table S1). The urban and agricultural watersheds water
250 samples have a higher alkalinity and ionic strength since their pedology is dominated by
251 carbonate soils (Table S1). It's also noteworthy that DOC concentrations of urban waters are
252 close to that of forested ones, but with much smaller seasonal variations. Those values are
253 within the range of values previously recorded and are characteristic of Seine River watershed
254 waters [29,301].
255
256 Table 2: Average (range) of some physicochemical properties of three catchment waters.
257 Original data taken from *Wang et al. (2020) (Table S2 in supplementary information [25])*.

	Forested water	Agricultural water	Urban water
pH	7.1 (6.3-7.7)	7.8 (7.1-8.8)	8.4 (8.0-9.0)
Conductivity (µs/cm)	247 (195-320)	666 (527-777)	1117 (877-1270)
DOC (mg/L)	5.6 (3.4-9.1)	3.5 (2.5-4.7)	5.2 (4.4-6.1)
Alkalinity (µM)	885 (661-1072)	3659 (2260-4663)	4457 (3397-5299)

3.2 Concentration of NPs-TiO_2 detected in three catchments

By comparing sp-ICPMS data for the ultrafiltered water (< 1 kDa) and the raw water, we can confirm the presence of NPs-TiO_2 in sampled waters (Fig. S1). The detected NPs-TiO_2 particle number concentration (PNC) ranges from 9×10^8 to 9×10^{10} particle L^{-1}, with an average value of 2×10^{10} particle L^{-1}. The mass concentration corresponds to a range of 0.5 to 70 µg NPs-TiO_2 L^{-1}, using the ionic Ti calibration curve and the procedure given in [25] and in the supplementary information. Few field data of NPs-TiO_2 in surface waters are available in literature (Table 3). Despite the variability in these reported literature values, we found higher values for the PNC of NPs-TiO_2 in the catchments. This difference can be attributed to the nature of sampling site (i.e., small watersheds vs larger rivers), sample preparation, and for the larger part most probably related to the sp-ICPMS analysis data processing. Indeed, given the very low concentration of dissolved Ti (i.e. 50 ng Ti L^{-1}), consistent with the thermodynamic solubility data of TiO_2 [41], a different data treatment method could be applied. This method is based on the subtraction of the background ion counts of the ultrafiltered matrix (< 1 kDa)

from those of the bulk sample to calculate PNC [25] (supplementary information section gives details on its validation as well as reference [25]). With this method, the smallest Ti-containing particles, which are usually eliminated as part of the so-called dissolved background by classical data treatment [39], are now measured. Additionally, as a result of using this new procedure, the measured NPs-TiO_2 PNC covers a wider size distribution. The data treatment impacts the mass concentration measurement only slightly, since very small particles account only for a small part of the NPs-TiO_2 mass concentrations. The mass concentration measured in this study covers a broad range with an average value equal to 11 µg NPs-TiO_2 L^{-1}, slightly higher than previously published values (Table 3). In addition, the different geological setting of these sites may also account for such differences, since NPs-TiO_2 PNC or mass concentration can be the result of past and/or present, natural and/or other anthropogenic inputs, mostly arising from the influence of agricultural practices on erosion fluxes taking place within the watersheds [1].

Table 3: Concentrations of NPs-TiO_2 measured in surface water from the literature and this study. n.g.: not given. n.a.: not analysed. *Ti: total content of filtered fraction after digestion. ** Engineered nanoparticles only as defined in [24].

Study site	Sample analysis	Range/Average 10^8.particle L^{-1}	Range/Average µg *NPs-TiO_2* L^{-1}	Reference

UK (Rural, Agricultural and Urban rivers)	< 0.45 µm digestion ICPMS	n.a.	0.55 - 6.48/2.1*	[51]
Austria (Old Danube Lake)	Unfiltered sp-ICPMS + ultrasonication	0.01 - 0.2/n.g.	n.g./1.7	[8]
USA (Missouri River)		n.g./4.4	n.g./2.2	[21]
Netherlands (Ijssel and Meuse Rivers)		0.05 - 1.5/ n.g.	0.2 - 8.1/ 3.1	[22]
China (Lake Taihu)		0.148-12/2.5	0.1-10	[26]
USA (Salt, truckee rivers & Clear Creek)		0.22-3.2/n.g.	2-42	[42]
USA (Crane, Stoop and Gills Creeks, South Carolina)	Treated $Na_4P_2O_7$ sonicated and centrifuged TOF-ICPMS	0.05-7.15/4.4	1-95/25**	[24]
France (Forested, brook)	**Unfiltered sp-ICPMS**	**60 – 720/280**	**3.5 - 23.4/10.2**	**This study**
France (Agricultural, stream)		**16 – 862/231**	**1.4 - 69.6/21.1**	
France (Urban, stream)		**9 – 39/27**	**0.5 - 5.9/3.1**	

291

292

293 Our results show that when looking only at our **urbanized watershed** (Table 3), all samples
294 are in the range of mass concentration reported in the literature. This study provides the first
295 dataset of NPs-TiO_2 in aquatic environment under different land-use in France. However, for
296 the most recent man-made nanoparticles production estimations [4] the mean concentration
297 of en-TiO_2 in European surface waters was estimated at 2.17 µg en-TiO_2 L^{-1}. Our value for NPs-
298 TiO_2, in the **urban watershed** is within this range but the total amount of TiO_2 (obtained by
299 acid digestion and ICP-MS analysis) in those water samples is much higher (see section 3.3 in
300 this paper). These NPs-TiO_2 concentrations are much lower than values corresponding to en-
301 TiO_2 only concentrations that can go up to 95 µg en-TiO_2 L^{-1} as detected with a specific sample
302 pre-treatment targeting a large recovery of engineered TiO_2 [24].
303
304 The **agricultural and forested stream samples** have a wider mass concentration range with
305 an upper value of 69.6 µg NPs-TiO_2 L^{-1}. This finding is not very surprising because in our study
306 the TiO_2 contributions from the natural geological background or other anthropogenic
307 activities (construction, agriculture…) are taken into account. However, it is to be noted that
308 higher simulated concentrations equal to 16 and 24.5 µg en-TiO_2 L^{-1} have been reported
309 [43,44].
310
311 Concerning the **differences between the three watersheds**, we can see that regardless of the
312 time of the sampling, the urban stream samples always contain less NPs-TiO_2 than the stream
313 samples from the other two watersheds either as NPs-TiO_2 number (Fig. 2) or mass
314 concentration (Fig. S6). The high values also reported for the forested watershed samples
315 could be due to naturally occurring NPs-TiO_2 since natural concentrations of colloids and
316 nanoparticles largely exceed that of engineered nanoparticles [45,15]. Likely causes are high

317 concentrations of Ti in soils from Northern Europe combined with high anthropogenic erosion
318 rates, which generate larger amounts of nanoparticles [14,46].
319
320 Looking at the **three watersheds individually**, some temporal trends for NPs-TiO_2
321 concentrations are observed (Fig. 2). A seasonal variability is detected for stream water
322 samples taken in the forested and agricultural watersheds. In the forested catchment, NPs-
323 TiO_2 concentrations increase from winter to spring, and then remain relatively constant. A
324 similar trend is observed for the agricultural catchment samples, but the highest
325 concentrations are measured in summer. These trends could be linked to supply-depletion
326 issues in the soils or the sediments. Under such situation, the highest PNC could be expected
327 during the rising stage of these small sub-basins (< 20 km^2) might have the highest PNC when
328 supply-depletion is minimal and dilution potential is small. This effect could be combined with
329 seasonal farming activities to affect the temporal distribution of the PNC for the agricultural
330 catchment.
331
332 In contrast, the PNC of the NPs-TiO_2 in the urban catchment are less variable (Fig. 2). Firstly,
333 because the larger area (116 km^2) of this watershed could integrate the inputs of different
334 sources controlling the PNC throughout the year. Secondly, this larger stream would allow a
335 more efficient combination of different processes contributing to the stabilization of the PNC
336 values with time. Thirdly, a more diffuse source of NPs-TiO_2 resulting from the constant wash-
337 off of TiO_2 particles used in common exterior paints and plasters on facades could reach
338 surface waters via urban transport pathways [47-50]. It is worth noting that no correlations of
339 NP-Ti concentrations were found with meteorological conditions parameters (rainfall
340 amounts, wind speed, temperature, humidity, cloud cover from https://www.historique-

341 meteo.net/france/ile-de-france/) during / before the sampling campaigns limiting our
342 understanding of the role played by those meteorological drivers (Table S8).
343

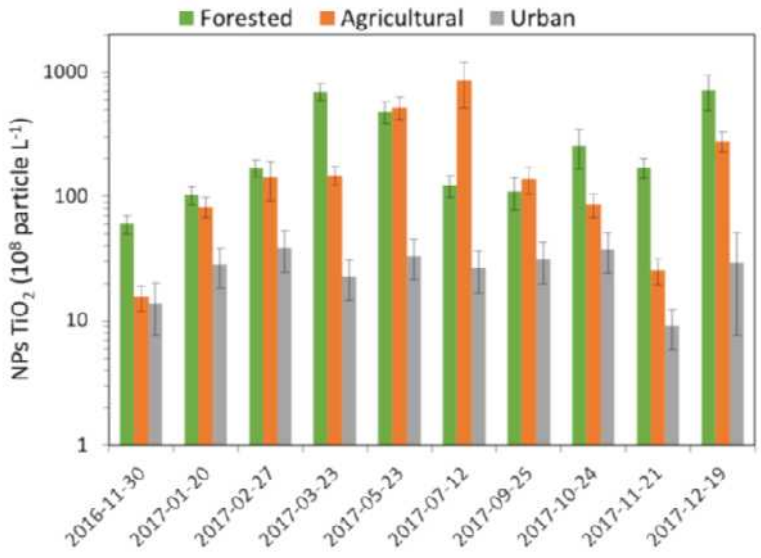

344

345 Figure 2: Particle number concentration (PNC) of NPs-TiO_2 measured at the three sites during
346 one-year of sampling. Samples were taken once per month, except for three months which
347 are missing.
348

349 3.3 Speciation and distribution of Ti

350 The dissolved (fraction < 1 kDa) and total Ti after acid digestion were quantified by ICPMS and
351 their concentrations together with NPs-TiO_2 are given in Table S7 and Fig. 3. The dissolved Ti
352 concentration ranges from 11 to 93 ng Ti L^{-1} with an annual mean value of 35, 39 and 56 ng Ti

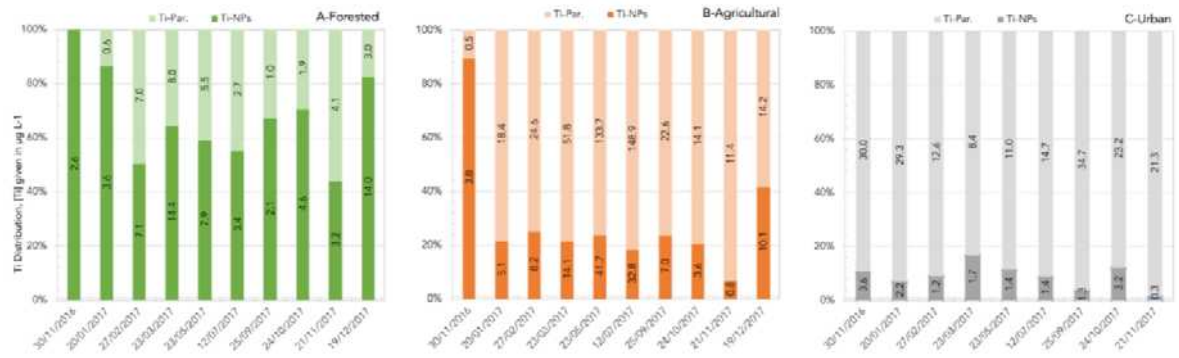

353 L^{-1} for forested, agricultural and urban catchments, respectively. Using current
354 thermodynamic data [41] the calculated dissolved Ti concentrations are around 50 ng Ti L^{-1}
355 within the pH range of the stream water samples (Table 1), suggesting that solubility
356 equilibrium is reached in these stream waters. Other studies have reported higher
357 concentrations or [Ti] in < 1 kDa fractions sampled in rural, agricultural and urban/industrial
358 rivers (i.e., 290 to 4650 ng Ti L^{-1}) [51]. Clearly more data on NPs-TiO_2 solubility and the
359 potential role of organic ligands that could increase Ti solubility are needed to better
360 understand both results. This dissolved fraction accounts on average for only 0.5%, 0.3% and
361 0.3% of the total Ti measured in bulk water samples (i.e., after total mineralization) from the
362 forested, agricultural and urban catchments, respectively and these small values are not
363 displayed in Fig. 3.

364 **Figure 3**: Ti distribution (%) of total Ti for two fractions i.e., the ***NPs-TiO_2*** fraction (Ti-NPs) and
365 large particles (Ti-Par) in three waters for one-year sampling, in which Ti-Par = Ti total – Ti NPs
366 – Ti dissolved with Ti dissolved less than 1% of tot. Panel A, B and C showing the data of the
367 forested, agricultural and urban watersheds, respectively. The numbers inserted in each bar
368 correspond to the mass concentration given in µgTi L^{-1} of measured Ti-NPs and calculated Ti-
369 Par.

370

371 The total amount of Ti obtained by acid mineralization (Table S7), for the three watersheds,
372 ranges from 2.1 to 181.7 µg Ti L^{-1}. In Fig. 3, Ti distributions of different fractions is given in %
373 of total Ti. On average, the NPs-Ti fraction (obtained by spICP-MS) represents 70%, 30% and
374 9% of the total Ti for the forested, agricultural and urban catchment samples, respectively.
375 Using the average concentration of Ti in suspended matter (SPM) (i.e. 2942 mg kg^{-1} SPM), and
376 the range of SPM content in the Seine river [29-31], the calculated Ti concentrations from

suspended matter would range from 6 to 495 µg Ti L^{-1}, showing that there is clearly a large reservoir of Ti in the SPM, in the range of the measured Ti-Par fraction (Fig.3). These results are different from previous findings [51] showing that 79% of Ti is colloidal for rural areas and 28% for urban rivers, then again, in [51] authors focused on the filterable fraction and not on the total Ti that includes particulate Ti and NPs-TiO_2 [51]. The filtration cut-off (i.e., < 0.45 µm) most probably stopped a large part of the NPs-TiO_2 [8], as in the case of Ag NPs [23,25]. The difference between the sp-ICPMS measure of Ti mass concentration and the total Ti concentration (illustrated in Fig. 3) also shows that a large amount of Ti is not detected by sp-ICPMS and is likely present in the form of larger homo or hetero aggregates that cannot be detected or quantified by this technique.

Assuming that the Ti detected in the NPs is present as TiO_2, an equivalent spherical TiO_2 diameter can be calculated using the bulk density of TiO_2 (4.23 g cm^{-3}). In Fig. 4, we can see that the average size of the TiO_2-NPs is smaller than the previously reported literature values [21,24,26,42]. This result may indicate that particle size may vary regionally. However, we believe that the data treatment (subtraction method) has a greater effect on the particle size distribution calculation. Some investigators use manufacturers' software [21,42] but the corrections applied to estimate the background may differ even with the same software [21,42] preventing direct comparison. Others use home-made spreadsheets or software [17,22,25] with no general consensus as to how to assign a size cut-off (3$\boldsymbol{\sigma}$, 5 $\boldsymbol{\sigma}$, frequency histogram subtraction). Another reason for the discrepancy is the sample pre-treatment before sp-ICPMS analysis and deviation mays also arise because particles are not spherical [17]. Some publications use sonication but with different frequencies and duration that again prevent direct comparisons (26,42), others researchers have also not sonicated the sample

while others use complex extraction protocols [24] and some even use pre-filtration [26]. This means that the community of scientists using sp-ICPMS should reach a consensus on how to treat the samples and the data or at least to have a common protocol to test their data treatment that will allow intercomparison between publications.

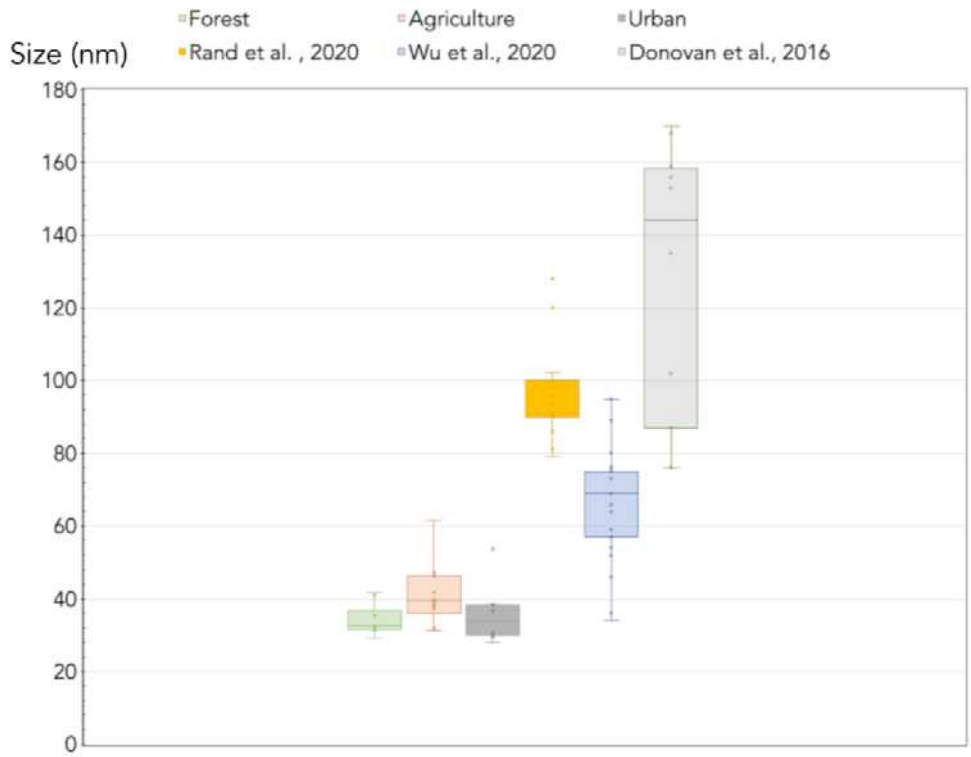

Figure 4: Calculated diameters of the TiO_2-NPs detected by sp-ICPMS and comparison with recently published data (see supplementary section for detailed size calculation procedure). [21]: Donovan et al., 2016; [26]: Wu et al., 2020; [42]: Rand et al., 2020.

3.4 Ti-bearing particles by SEM-EDX analysis

The SEM imaging and EDX analyses were performed to qualitatively confirm the presence of the NPs-TiO_2 detected by sp-ICPMS and to characterize their size, morphology, and elemental composition. The observed particles differ in shape and size (Fig. 5 and Fig. S9), ranging from nanoscale up to several micrometres, in the form of either individual particles or hetero-aggregates/agglomerates in agreement with the data of Fig. 4. Moreover, most detected

particles are found associated with other elements, such as Al, Si, K, Ca, Fe. Their coexistence with Ti reveals that they are most probably naturally occurring particles, derived from ilmenite ($FeTiO_3$) and clay minerals [52]. These observations are in agreement the results given in Fig. 3 showing that a large part of Ti is not present as NPs-TiO_2 but as larger objects. A recent study proposed that the morphology of TiO_2 particles and their status in unperturbed mineral–organic assemblages may provide insights on their source [53]. Our observations (Fig. 5 and Fig. S9) are not sufficient to come to the same conclusion. Moreover, observations could be undermined by sample storage as stated in [53]. Our findings are, however, similar to the ones reported for pure and Ti rich hetero-aggregates [24,26,42].

Although SEM-EDX cannot provide a quantitative measurement of Ti speciation, a few pure TiO_2 nanoparticles, that could correspond to en-TiO_2 as identified by [24], were detected suggesting but not confirming some anthropogenic origin. In addition, these images can help us to understand why sp-ICPMS failed to detect larger aggregates. Indeed, during the nebulization step, a size fractionation could occur sending the largest particles (> 5 µm) to the drain [54]. The ionization efficiency of a single NPs-TiO_2 would also not be the same as that of the same NPs-TiO_2 imbedded in a much larger hetero-aggregate composed of oxides and clays and organic matter. To our knowledge no one has examined those effects for sp-ICPMS measurements.

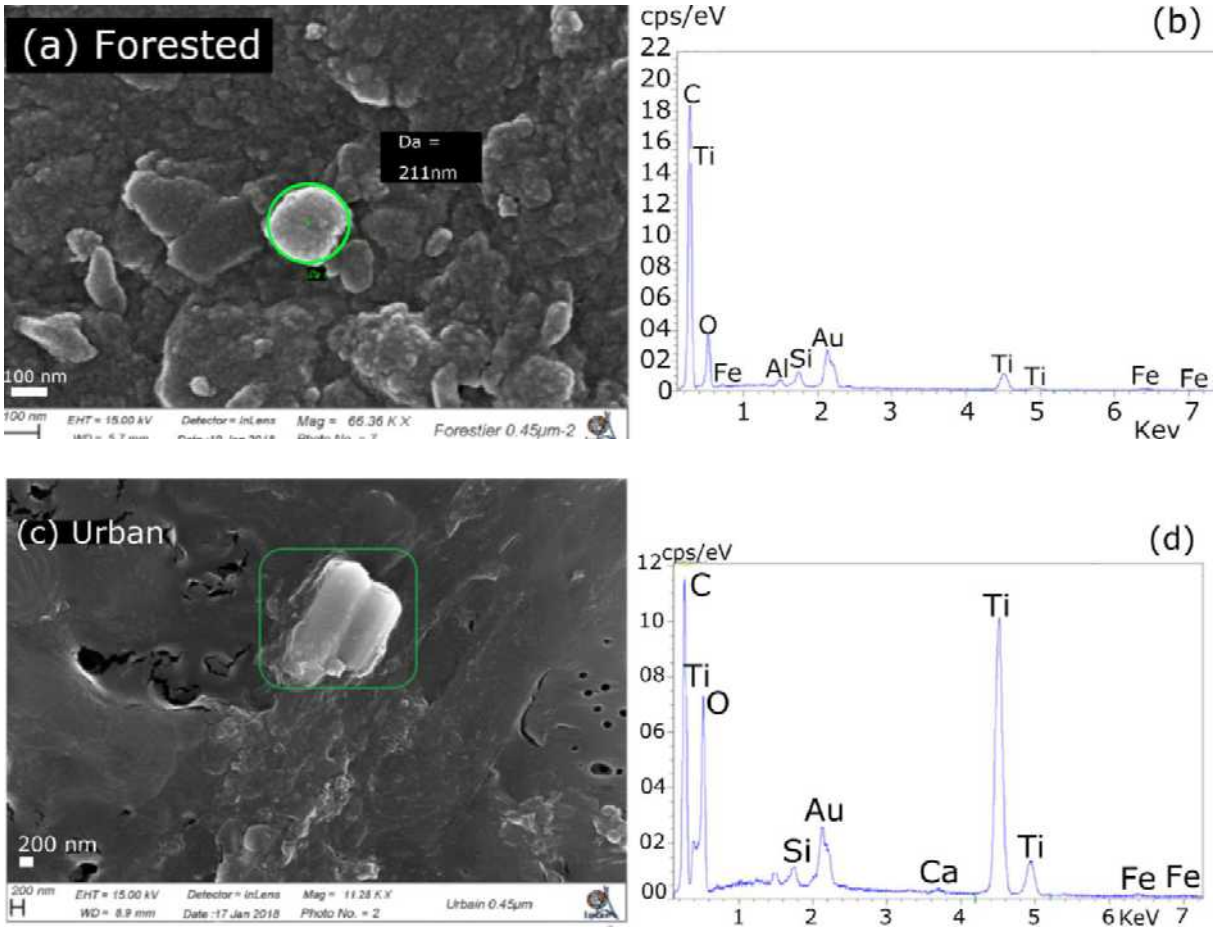

Figure 5: Left: SEM images of filters retaining suspended particles containing TiO_2, with different shapes, present in sampled waters. Panels (a) and (c) showing a sample from the forested and urban watersheds, respectively. Right: Panel (b) and (d) showing the EDX analysis of corresponding particles highlighted by the green circle in panel (a) and the green square in panel (c).

Keeping in mind the limitation of the above approaches our observations raise a series of questions. Why do the agricultural and forested samples have much higher NPs-TiO_2 concentrations (both PNC and mass concentration) than the urban watershed samples? Is this difference due to source and/or related watershed processes related to one another? Can we estimate land-use specific export rates using the present data set?

3.5 Biogeochemical factors controlling NPs-TiO_2 in three watersheds.

Correlation between elements and NPs-TiO_2 concentrations (i.e., number or mass) can be interpreted within a mass balance approach or used to identify driving parameters or processes for small watersheds [55]. It should be noted that the correlation coefficient r, together with p-value are evaluated. With $r \geq 0.77$ and p-value ≤ 0.05 significant at the 95 % confidence level, the correlation is considered statistically significant [56]. In addition, the absence of correlations between the NPs-TiO_2 PNC, mass concentration, any other metal ions and anions, especially chloride ions, suggests that dilution is not responsible for the trends that are subsequently discussed. In fact, if NPs-TiO_2 concentrations were a result of varying degrees of dilution of the soil water entering the streams, background electrolytes (i.e. Cl^-) concentrations would likely covary. No such covariation or correlation was observed.

Our previous study on the same watersheds demonstrated a strong positive correlation between DOC concentrations and silver nanoparticles concentration (i.e. [Ag-NPs]) reflecting the control of the dissolved organic matter (DOM) on the number and mass concentration of Ag-NPs [25]. The more DOM, the more Ag-NPs were detected, although this occurs mainly in the forested water samples.

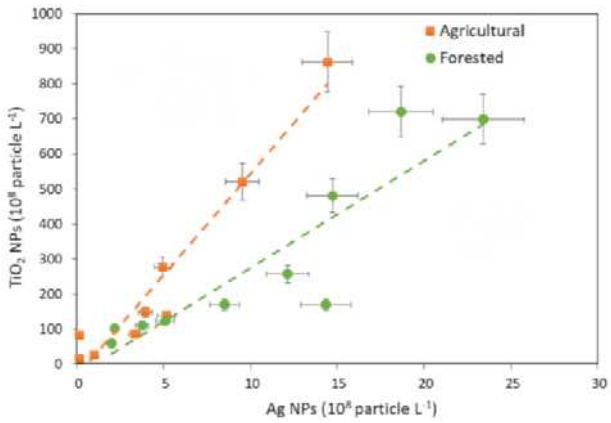

Figure 6: Particle number concentration (PNC) of NPs-TiO_2 as function of that of Ag NPs in agricultural and forested watersheds. Ag-NPs concentrations are from [25]. The correlation coefficients r corresponding to Agricultural orange and Forested green broken lines are equal to $r_{Agricultural}$ = 0.96 and $r_{forested}$ = 0.89. Their corresponding *p* value are equal to 0.00003 and 0.0004 for a sampling size n=9 and 10, respectively.

Positive correlations with $r \geq 0.89$ are observed between the Ag-NPs PNC and the NPs-TiO_2 PNC for the agricultural and forested catchments (Fig. 6). Consistently, for the forest water samples, a strong positive correlation (r = 0.91) between NPs-TiO_2 and DOC concentrations is observed (Fig. 7). Like for silver [25], it would be evidence of dynamic control of DOM on NPs-TiO_2 in this watershed. The stabilization effect of DOM mainly accounts for this trend and it has been reported in simplified and relevant freshwater matrix [57-60]. DOM can suppress the dissolution/aggregation processes by electrostatic repulsion, steric stabilization and hydrophobic interaction. This could also explain the high fraction of total Ti (i.e. 70%) detected as NPs-TiO_2 in the forested catchment. This can cannot be explained by dilution because if the range in NP-TiO_2 concentration was the result of varying degrees of dilution of the soil water entering the streams, variations in background electrolytes (i.e. Cl^-) would likely covary. In addition, it cannot be explained by the effect of any metrological drivers that would lead to high runoff of all constituent from soils including organic matter and its associated NPs-TiO_2 [25].

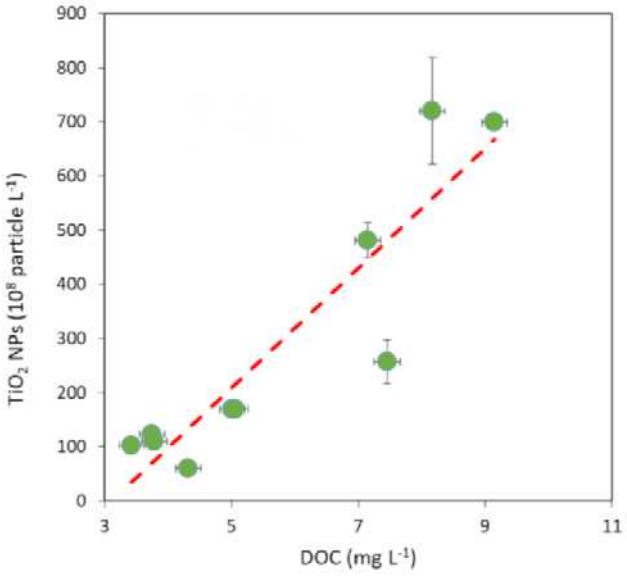

Figure 7: Mass concentration of NPs-TiO_2 as function of DOC concentration in water samples from the forested watershed. The correlation coefficient r corresponding to the orange broken line is equal to r = 0.91 and it corresponds to a p value equal to 0.0002 and a sampling size n=9

There is no obvious trend in NP-TiO_2 concentration with DOC for the agricultural stream samples. Other factors, such as ionic strength, may also partly control the fate of the NPs-TiO_2 in this watershed. A negative trend between NPs-TiO_2 and conductivity (r = 0.77) (Fig. S7) is reported. A higher ionic strength and higher divalent cations concentrations favour the aggregation/flocculation of NPs-TiO_2 [58, 61-62]. The decreasing NPs-TiO_2 concentration therefore most likely results from the enhanced aggregation by the increasing IS and divalent cations concentrations. Such effect of IS on aggregation is associated with the compression of the diffuse layer and decreasing of surface charge [62]. Under the field pH range, NPs-TiO_2 should have a negative charge according to their Point of Zero Charge (i.e., 6.5 or 4.5 for anatase or rutile, respectively), the presence of higher divalent cations electrostatically bound to the negatively charged NP-TiO_2 would favour an increase (i.e. going from negative values to less negative ones or even positive values) in zeta potential of the NPs-TiO_2 [63].

In urban stream samples, since DOC, IS and cations concentrations barely vary, there is no clear relationship between the NPs-TiO_2 PNC or mass concentration associated with these factors. Moreover, the fraction of Total Ti under the form of NPs-TiO_2 is very small (9%), it is therefore difficult to discuss processes affecting the NPs-TiO_2 even if the SEM images clearly show that part of the total Ti is in the form of aggregates of smaller objects (Fig. 5, Fig. S9). Caution must be taken when interpreting the observations made by SEM-EDX on filtered samples since the observed aggregates could be artefacts caused by filtration. Large objects above 100 nm are however observed (Fig. 5, Fig. S9) and will be part of the total Ti pool. Remarkably, the average percentage of the total Ti under the form of NPs-TiO_2 for each watershed is negatively correlated ($r = 0.98$) to the average conductivity measured for each watershed (Table S7) suggesting that similar processes are at work in the three watersheds favouring their transfer in the particulate fraction by aggregation of smaller NPs-TiO_2 with other colloids such as clays or organic matter [64-67].

In addition to process indicators discussed above, the correlation between NPs-TiO_2 and other elements can be used to identify the potential sources of NPs-TiO_2. First, the global Seine river watershed has a long historical record of pollution lasting from more than 300 centuries [68,69]. Speleothems in Paris record the historical pollution of Pb, V, Cu, Cd due to the increased urbanization of Paris mega city [68]. In the Orge river catchment (close to the studied catchments), with a contrasted land-use pattern (forested, agricultural and urban areas), trace elements (Pb, Zn, Cu and Sb) concentrations are drastically elevated in the SPM fraction due to urbanization of the catchment, as urban run-off and sewage strongly influence the river geochemistry [69,70]. The main sources of the pollution in the catchment are:

530 atmospheric emissions due to individual and industrial combustion release, erosion of run-off
531 of urban surfaces (building walls, roofs, roads) and remobilization of historical deposits by
532 resuspension of bottom sediments [70,71]. A previous study, concluded that Cu, Pb, Sb and
533 Zn were urban trace elements, while Cr, Co and Ni were more closely related to alumino-
534 silicates sources [70].
535 The influence of pollution affecting the geochemistry and the total content of elements in the
536 collected stream samples can be assessed by calculating the annual average enrichment factor
537 (EF) [72,73].
538 One reference material was used in this study, a Seine riverbed sediment (SRBS) collected N
539 48° 24' 39", E 3° 24' 05" at Fontaine, France [73] before the river enters the anthropogenically
540 impacted area of the Région île de France including Paris mega city where the studied
541 watersheds are located (Fig. 1). EF[Me] values are given in Table 4 for Cd, Pb, Ni, Cu, Zn, Sb
542 and As. The urban catchment samples are the only ones that have significant EF values
543 indicating contamination (i.e. EF > 2 [74]) for all elements, even Ni which was associated more
544 closely related to alumino-silicates rather than urbanization [70]. However, a part of the
545 watershed is covered by agricultural activities that could account for an EF[Ni] > 2 because of
546 increased soil erosion due to agricultural practices [1] (Fig. 1). This means that on average for
547 the forested and agricultural sites the influence of anthropogenic activities is not seen even if
548 sewage sludge is dispersed on the soils because of a higher natural background signal. This
549 conclusion would also stand for the NPs-TiO_2 (including en-TiO_2) introduced by biosolids that
550 are used for agriculture [75].
551
552 Table 4: Average enrichment factor (EF) of selected elements in three small catchments
553 normalized to suspended matter particles (SRSM) of Seine River.

	Cd	Pb	Ni	Cu	Zn	Sb	As
Forested	2.0	0.3	2.5	1.0	0.9	2.2	2.4
Agricultural	1.5	0.9	1.6	1.8	0.7	4.8	4.2
Urban	6	6	8	11	20	40	8

Another mean of tracking the source of the NPs-TiO_2 is to look for correlations between NPs-TiO_2 concentration and bulk content of elements linked to natural or anthropogenic sources. This is valid especially in the case of the forested and agricultural watersheds samples since NPs-TiO_2 account for 70% and 30% of the total Ti on average, respectively.

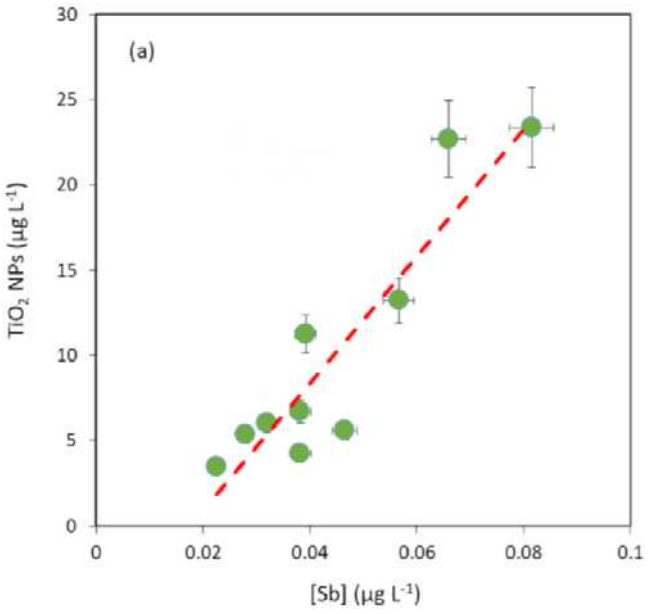

562

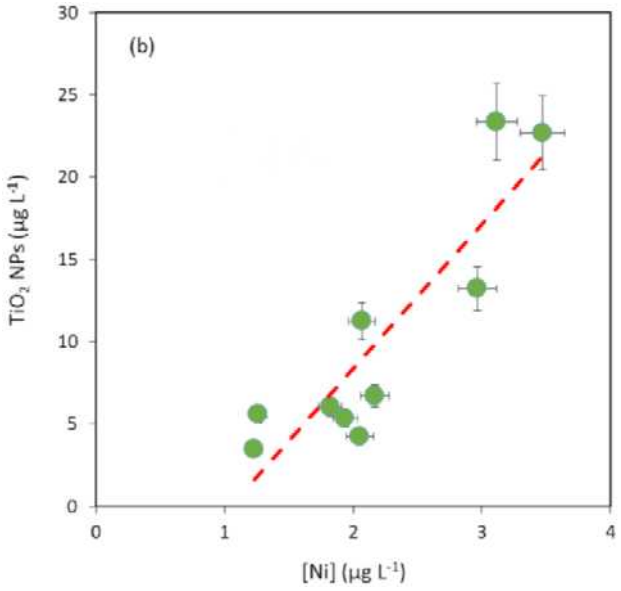

563

564

565 Figure 8: Mass concentration of TiO_2 NPs as function as that (bulk minus dissolved) of (a) Sb

566 and (b) Ni in forested water. The correlation coefficients r corresponding to the orange broken line are

567 equal to r = 0.91 and r = 0.89 in panel (a) and (b), respectively. They correspond to a p value equal to 0.0002 and

568 0.0005 with a sampling size n=10.

569

570 In Fig. 8, strong correlations are observed between NPs-TiO_2 and Sb and Ni for the forested

571 catchment samples. *Lepape et al.* [70] concluded that Ni is more closely related to alumino-

572 silicates sources: this could mean that our correlation is pointing towards a natural source for
573 the NPs-TiO_2 in this watershed. The other explanation, suggested by the correlation with Sb
574 (Fig 8a) is that a similar process controls the fate of both elements and the NPs-TiO_2. Here
575 organic matter binding for Sb [75-77] or stabilization of natural clays for Ni are realistic
576 processes that would generate such trends since a very strong correlation is seen with NPs-
577 TiO_2 and DOC (Fig. 7).
578
579 In the case of the agricultural catchment samples the correlation is strong with As, Zn and Ni
580 (Fig. S8)
581 Only Sb and As have an EF > 2 which could be related to inputs by an external source like
582 biosolid application. These trends cannot be explained by dilution, no correlation with Cl^- ions
583 is found [25], or with metrological drivers that would lead to high runoff of all constituent
584 from soils including trace metal pollutants and the associated NPs-TiO_2 [78] it is most probably
585 the erosion controlled by agricultural processes [46,78] that accounts for the release of NPs-
586 TiO_2.
587
588 When it comes to urban stream water samples, no clear correlations, between NPs-TiO_2 and
589 elements from anthropogenic origin, are seen. The small amount of total Ti in the form of NPs-
590 TiO_2 explains this lack of correlation. This smaller contribution of the NPs-TiO_2 pool to the bulk
591 Ti could be the consequence of the instability of the NPs-TiO_2 aggregates from different
592 sources as well as the variability of hydrological factors along the flow as NPs-TiO_2 are
593 transported downstream of effluent sources [51,65,66]. Despite the difficulty in identifying all
594 potential sources (natural vs anthropogenic contamination for all three watersheds), the
595 effect of land-use can be addressed by calculating the normalized fluxes that can be obtained

by integrating the monthly river discharge volume of each sampling period and the respective watersheds areas.

3.6 Exportation flux of TiO_2 from each watershed

The normalized export-rates calculated as mass of Ti species are given in Fig. 9. For NPs-TiO_2, the agricultural watershed has the highest average value equal to 0.8 kg Ti $year^{-1}$ km^{-2}, with a significant temporal variability. Forested and urban catchments have similar export-rates, which are respectively 0.3 and 0.4 kg Ti $year^{-1}$ km^{-2}. When compared to our calculated normalized export rates for the Ijssel and Meuse rivers, 10.9 kg Ti $year^{-1}$ $km^{-2}$and 0.8 kg Ti $year^{-1}$ km^{-2}, respectively, we are in the same range and closer to the one obtained for the Meuse river. Interestingly, the Ijssel watershed is characterized by intensive agricultural practices with croplands covering 70% of the basin and has the highest normalized export-rate of NPs-TiO_2, much like our much smaller agricultural watershed [28]. These results clearly show that agricultural practices have a different impact on NPs-TiO_2 export than the other land-use types either because of specific processes occurring in the watershed or specific sources associated with fertilizer use or application of biosolids. It was demonstrated, for instance in the Meuse River [27], that soil erosion by agricultural management practices favoured the transfer of terrestrial organic matter and therefore associated NPs-TiO_2 via the suspended particulate matter.

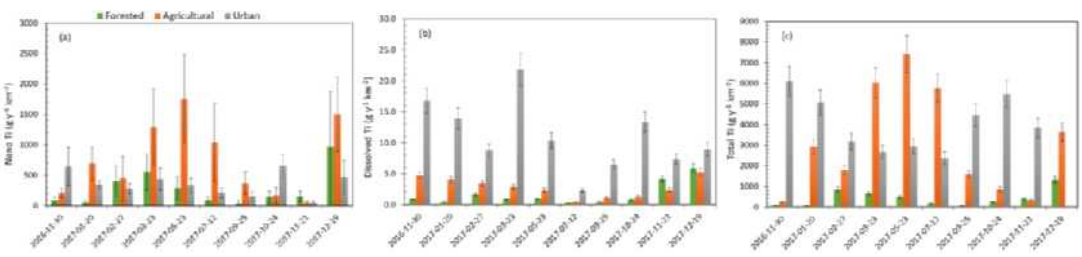

Figure 9: Export-rate of (a) nanoparticulate (b) dissolved < 1 kDa (c) total Ti detected in three waters along the sampling year.

For dissolved Ti, the urban stream has a higher average export rate equal to 11.0 g Ti $year^{-1}$ km^{-2} than forested and agricultural stream with respective export rates equal to 1.6 and 2.8 g Ti $year^{-1}$ km^{-2}. The same trend is calculated for total Ti export, equal to 4.0, 3.0 and 0.4 kg Ti $year^{-1}$ km^{-2} for urban, agricultural and forested streams, respectively. If we look at the calculated export rates along the year of sampling, the forested and agricultural watersheds clearly show a similar temporal variation with high export fluxes for the NPs-TiO_2 in the warmer months while the highest export rates are observed in the cold months for the dissolved fraction (Fig. 9). This could be due to the much smaller size of those two watersheds, which therefore have a much higher reactivity under changing meteorological or hydrological conditions. In the warmer months the NPs concentration would increase due to lower water flow but increased management practices (agriculture or forestry). No clear trend is observed for the urban watershed with meteorological or hydrological stages. It suggests that in this larger catchment sources and processes affecting Ti in general are more complex and that the variability of hydrological factors along the flow modifies them downstream of effluent sources.

These output fluxes can be compared to estimated output of Ti. For instance, for France annual soil loss by erosion on arable land is equal to 200 tons of soil $year^{-1}$ km^{-2} [46]. This corresponds to an output flux of 628 kg Ti $year^{-1}$ km^{-2} using an average concentration of Ti in agricultural soils in France equal to 3.11 g Ti kg^{-1} [14]. The present estimations demonstrate that most part of outgoing fluxes are not in the form of NPs-TiO_2 but rather in the form of

larger particulate (i.e. > 100 nm) or homo or hetero-aggregates, as seen in this work (Fig. 5) and previous studies [24,53].

Conclusions

NPs-TiO_2 have been identified in creek waters from three small sub-basins. The highest concentrations occurred in forested and agricultural catchments. For the former, it is mostly due to the high natural background, biogeochemical activity, and conditions that favours stable NP-TiO_2. For agricultural watershed, it is likely related to seasonal farming practices and erosion controlling TiO_2 from natural sources mostly. Moreover, environmental processes controlled by DOC, IS, and divalent cations have been identified in real-world natural systems, suggesting the complexity of the fate of NPs-TiO_2 in aquatic systems influenced by diffuse sources, like in the urban catchment. A similar process and fate of other engineered nanoparticles could be expected since TiO_2 can potentially serve as sentinel because of its long-history and large commercial use. Regarding the unexpected lower concentration of NPs-TiO_2 present in urban water, it's very likely related to the aggregation/flocculation/sedimentation that can help large particles/aggregates to be removed from the surface water layer that was sampled in this study, resulting in short residence time of discharged NPs-TiO_2. Additionally, microscopy imaging confirmed the presence of NPs in the three catchments. Furthermore, the land-area normalized annual flux of NPs-TiO_2 (1.65 kg TiO_2 $year^{-1}$ km^{-2}) was highest for the agricultural catchment, suggesting that agricultural practices have a different impact on the NPs-TiO_2 dynamics and exports than other land-uses (urban or forestry). A similar trend is also found by the reanalysis of recent literature data.

In the future anthropogenic nanoparticles will be continuously produced, distributed and rival the amount of naturally occurring nanoparticles. Therefore, further studies and measurement of NPs-TiO_2 need to be performed in suspended matter, sediments and soils to better characterize their origin and fate. Given that the introduction of nanotechnology-derived NPs is a more recent event that natural NPs, the issue of anthropogenic nanoparticles in natural system is more likely dynamic. New survey with state the art techniques like TOF-sp-ICPMS, which provides a multiple element analysis for each NPs, will allow a better understanding their impacts and fate on longer time scales.

Acknowledgements

This project has been supported by Ile de France Region through the DIM Analytics program (Convention ESPCI-RVT-IPGP-N°2015-3). Part of this work was supported by grants from Région Ile-de-France R2DS and PIREN Seine programs. Parts of this work were supported by IPGP multidisciplinary program PARI, and by Paris–IdF region SESAME Grant no. 12015908. This study contributes to the IdEx Université de Paris ANR-18-IDEX-0001. Professor Jim Ranville is greatly acknowledged for proof reading the English but mostly for very helpful editorial suggestion to improve the present article.

683

684 References

685 1 Sen, I.S., Peucker-Ehrenbrink, B., 2012. Anthropogenic disturbance of element cycles
686 at the earth's surface. Environ. Sci. Technol., 46, 8601-8609.
687 https://doi.org/10.1021/es301261x

688

689 2 Sang, L., Zhao, Y., Burda, C., 2014. TiO2 Nanoparticles as Functional Building Blocks.
690 Chem. Rev. 114, 9283–9318. https://doi.org/10.1021/cr400629p

691

692 3 Jankovic, N., Plata, D. 2019. Engineered nanomaterials in the context of global element
693 cycles. Environ. Sci. nano. 6, 2697. https://doi.org/10.1039/c9en00322c

694

695 4 Sun, T.Y., Bornhöft, N.A., Hungerbühler, K., Nowack, B., 2016. Dynamic Probabilistic
696 Modeling of Environmental Emissions of Engineered Nanomaterials. Environ. Sci. Technol. 50,
697 4701–4711. https://doi.org/10.1021/acs.est.5b05828

698

699 5 Picciono, F., Gottschalk, F., Segger, S., Nowack, B. 2012. Industrial production
700 quantities and uses of ten engineered nanomaterials in Europe and the world. J. Nanopart.
701 Res. 14, 1109-1120. https://doi.org/10.1007/s11051-012-1109-9

702

703 6 Kaegi, R., Boller, M., 2008. Synthetic TiO2 nanoparticle emission from exterior facades
704 into the aquatic environment. Environ. Pollut. 156, 233–239.
705 https://doi.org/10.1016/j.envpol.2008.08.004

706

707 7 Windler, L., Lorenz, C., Von Goetz, N., Hungerbühler, K., Amberg, M., Heuberger, M.,
708 Nowack, B., 2012. Release of titanium dioxide from textiles during washing. Environ. Sci.
709 Technol. 46, 8181–8188. https://doi.org/10.1021/es301633b
710
711 8 Gondikas, A.P., Von Der Kammer, F., Reed, R.B., Wagner, S., Ranville, J.F., Hofmann, T.,
712 2014. Release of TiO2 nanoparticles from sunscreens into surface waters: A one-year survey
713 at the old danube recreational lake. Environ. Sci. Technol. 48, 5415–5422.
714 https://doi.org/10.1021/es405596y
715
716 9 Kaegi, R., Englert, A., Burkhardt, M., 2017. Release of TiO_2 – (Nano) particles from
717 construction and demolition landfill. NanoImpact 8, 73–79.
718 https://doi.org/10.1016/j.impact.2017.07.004
719
720 10 Weir, A., Westerhoff, P., Fabricius, L., Hristovski, K., Von Goetz, N., 2012. Titanium
721 dioxide nanoparticles in food and personal care products. Environ. Sci. Technol. 46, 2242–
722 2250. https://doi.org/10.1021/es204168d
723
724 11 Kiser, M.A., Westerhoff, P., Benn, T., Wang, Y., Pérez-Rivera, J., Hristovski, K., 2009.
725 Titanium nanomaterial removal and release from wastewater treatment plants. Environ. Sci.
726 Technol. 43, 6757–6763. https://doi.org/10.1021/es901102n
727
728 12 Polesel, F., Farkas, J., Kjos, M., Almeida Carvalho, P., Flores-Alsina, X., Gernaey, K. V.,
729 Hansen, S.F., Plósz, B.G., Booth, A.M., 2018. Occurrence, characterisation and fate of

730 (nano)particulate Ti and Ag in two Norwegian wastewater treatment plants. Water Res. 141,
731 19–31. https://doi.org/10.1016/j.watres.2018.04.065
732
733 13 Westerhoff, P., Song, G., Hristovski, K., Kiser, M.A., 2011. Occurrence and removal of
734 titanium at full scale wastewater treatment plants: Implications for TiO_2 nanomaterials. J.
735 Environ. Monit. 13, 1195–1203. https://doi.org/10.1039/c1em10017c
736
737 14 Reiman, C. de Caritat, P., GEMAS Project Team, NGSA Project Team, 2012. New soil
738 composition data for Europe and Australia: Demonstrating comparability, identifying
739 continental -scale processes and learning lessons for global geochemical mapping. Science of
740 the Total Environment 416, 239-252. https://doi.org/10.1016/j.scitotenenv.2011.11.019
741
742 15 Hochella M. F. Jr, Mogk D. W., Ranville J., Allen I. C., Luther G. W., Marr L. C., McGrail
743 B. P., Murayama M., Qafoku N. P., Rosso K. M., Sahai N., Schroeder P. A., Vikesland P.,
744 Westerhoff P. and Yang Y. (2019) Natural, incidental, and engi-neered nanomaterials and their
745 impacts on the Earth system. Science 363, eaau8299–12.
746
747 16 Wagner, S., Gondikas, A., Neubauer, E., Hofmann, T., Von Der Kammer, F., 2014. Spot
748 the difference: Engineered and natural nanoparticles in the environment-release, behavior,
749 and fate. Angew. Chemie - Int. Ed. 53, 12398–12419. https://doi.org/10.1002/anie.201405050
750
751 17 Tharaud, M., Gondikas, A.P., Benedetti, M.F., von der Kammer, F., Hofmann, T.,
752 Cornelis, G., 2017. TiO 2 nanomaterial detection in calcium rich matrices by spICPMS. A matter

753 of resolution and treatment. J. Anal. At. Spectrom. 32, 1400–1411.
754 https://doi.org/10.1039/C7JA00060J
755
756 18 Nowack, B., Baalousha, M., Bornhöft, N., Chaudhry, Q., Cornelis, G., Cotterill, J.,
757 Gondikas, A., Hassellöv, M., Lead, J., Mitrano, D.M., Von Der Kammer, F., Wontner-Smith, T.,
758 2015. Progress towards the validation of modeled environmental concentrations of
759 engineered nanomaterials by analytical measurements. Environ. Sci. Nano 2, 421–428.
760 https://doi.org/10.1039/c5en00100e
761
762 19 Lead, J.R., Batley, G.E., Alvarez, P.J.J., Croteau, M.-N., Handy, R.D., McLaughlin, M.J.,
763 Judy, J.D., Schirmer, K., 2018. Nanomaterials in the Environment: Behavior, Fate,
764 Bioavailability, and Effects An Updated Review. Environ Toxicol Chem, 37: 2029-2063.
765 https://doi.org/10.1002/etc.4147
766
767 20 Aznar, R., Barahona, F., Geiss, O., Ponti, J., José Luis, T., Barrero-Moreno, J., 2017.
768 Quantification and size characterisation of silver nanoparticles in environmental aqueous
769 samples and consumer products by single particle-ICPMS. Talanta 175, 200–208.
770 https://doi.org/10.1016/j.talanta.2017.07.048
771
772 21 Donovan, A.R., Shi, H., 2016. Single particle ICP-MS characterization of titanium dioxide,
773 silver, and gold nanoparticles during drinking water treatment. Chemosphere 144, 148–153.
774 https://doi.org/10.1016/j.chemosphere.2015.07.081
775

776 22 Peters, R.J.B., van Bemmel, G., Milani, N.B.L., den Hertog, G.C.T., Undas, A.K., van der
777 Lee, M., Bouwmeester, H., 2018. Detection of nanoparticles in Dutch surface waters. Sci. Total
778 Environ. 621, 210–218. https://doi.org/10.1016/j.scitotenv.2017.11.238
779
780 23 Yang, Y., Long, C-L., Li , H-P., Wang , Q., Yang, Z-G., 2016. Analysis of silver and gold
781 nanoparticles in environmental water using single particle-inductively coupled plasma-mass
782 spectrometry. Science of The Total Environment 563–564 (1), 996–1007.
783 doi:10.1016/j.scitotenv.2015.12.150.
784
785 24 Loosli, F., Wang, J., Rothenberg, S., Bizimis, M., Winkler, C., Borovinskaya, O.,
786 Flamignie, L., Baalousha, M., 2019. Sewage spills are a major source of titanium dioxide
787 engineered (nano)-particle release into the environment. Environ. Sci.: Nano, 2019,6, 763-777
788 https://doi.org/10.1039/C8EN01376D
789
790 25 Wang, J., Alasonati, E., Tharaud, M., Gelabert, A., Fisicaro, P., Benedetti, M.F., 2020.
791 Flow and fate of silver nanoparticles in small French catchments under different land-uses:
792 The first one-year study. 2020. Water Research Water Res 176, 115722.
793 https://doi.org/10.1016/j.watres.2020.115722
794
795 26 Wu, S., Zhang, S., Gong, Y., Shi, L., Zhou, B. 2020 Identification and quantification of
796 titanium nanoparticules in surface waters: A cases study in Lake Taihu, China. Journal of
797 hazardous Materials, 382, 121045.
798

27 Lambert, T., Bouillon, S., Darchambeau, F., Morana, C., Roland, F.A.E., Descy, J.P., Borges, A. V., 2017. Effects of human land use on the terrestrial and aquatic sources of fluvial organic matter in a temperate river basin (The Meuse River, Belgium). Biogeochemistry 136, 191–211. https://doi.org/10.1007/s10533-017-0387-9

28 Verwijmeren, J., Wiering, M., 2007. Many rivers to cross. Cross border co-operation in river management. Eburon Academic, Delft

29 Roy S., Gaillardet J. and Allegre C. J. (1999) Geochemistry of dissolved and suspended loads of the Seine river, France: anthropogenic impact, carbonate and silicate weathering. Geochimica Et Cosmochimica Acta 63, 1277–1292.

30 Bonnot, C., 2015. L'origine des métaux et la dynamique du zinc dans le bassin de la Seine. PhD, Université Paris Diderot, 205p.

31 Bonnot, C.A., Gélabert, A., Louvat, P., Morin, G., Proux, O., Benedetti, M.F., 2016. Trace metals dynamics under contrasted land uses: contribution of statistical, isotopic, and EXAFS approaches. Environ. Sci. Pollut. Res. 1–21. https://doi.org/10.1007/s11356-016-6901-0

32 Guo, L. and Santschi, P.H. (2007). Ultrafiltration and its Applications to Sampling and Characterisation of Aquatic Colloids. In Environmental Colloids and Particles (eds J. Buffle, H.P. van Leeuwen, K.J. Wilkinson and J.R. Lead). doi:10.1002/9780470024539.ch4

823 33 Degueldre, C., Favarger, P.Y., Rossé, R., Wold, S., 2006a. Uranium colloid analysis by
824 single particle inductively coupled plasma-mass spectrometry. Talanta 68, 623–628.
825 https://doi.org/10.1016/j.talanta.2005.05.006
826
827 34 Degueldre, C., Favarger, P.Y., Wold, S., 2006b. Gold colloid analysis by inductively
828 coupled plasma-mass spectrometry in a single particle mode. Anal. Chim. Acta 555, 263–268.
829 https://doi.org/10.1016/j.aca.2005.09.021
830
831 35 Degueldre, C., Favarger, P-Y., Bitea, C., 2004. Zirconia colloid analysis by single particle
832 inductively coupled plasma–mass spectrometry. Anal. Chim. Acta 518, 137–142.
833 https://doi.org/10.1016/J.ACA.2004.04.015
834
835 36 Degueldre, C., Favarger, P.Y., 2004. Thorium colloid analysis by single particle
836 inductively coupled plasma-mass spectrometry. Talanta 62, 1051–1054.
837 https://doi.org/10.1016/j.talanta.2003.10.016
838
839 37 Degueldre, C., Favarger, P.Y., 2003. Colloid analysis by single particle inductively
840 coupled plasma-mass spectroscopy: A feasibility study. Colloids Surfaces A Physicochem. Eng.
841 Asp. 217, 137–142. https://doi.org/10.1016/S0927-7757(02)00568-X
842
843 38 Mitrano, D.M., Lesher, E.K., Bednar, A., Monserud, J., Higgins, C.P., Ranville, J.F., 2012.
844 Detecting nanoparticulate silver using single-particle inductively coupled plasma-mass
845 spectrometry. Environ. Toxicol. Chem. 31, 115–121. https://doi.org/10.1002/etc.719
846

847 39 Pace H. E., Rogers N. J., Jarolimek C., Coleman V. A., Higgins C. P. and Ranville J. F. (2011)
848 Determining Transport Efficiency for the Purpose of Counting and Sizing Nanoparticles via
849 Single Particle Inductively Coupled Plasma Mass Spectrometry. Analytical Chemistry 83, 9361–
850 9369. https://doi.org/10.1021/ac300942m
851
852 40 BIPM, IEC, IFCC, ILAC, ISO, IUPAC, IUPAP and OIML, Guide to the Expression of
853 Uncertainty in Measurement, JCGM 100:2008 (GUM 1995 with minor corrections), 2008.
854
855 41 Schmidt, J., Vogelsberger, W., 2009. Aqueous long-term solubility of titania
856 nanoparticles and titanium(IV) hydrolysis in a sodium chloride system studied by adsorptive
857 stripping voltammetry. J. Solution Chem. 38, 1267–1282. https://doi.org/10.1007/s10953-
858 009-9445-9
859
860 42 Logan N. Rand, Yuqiang Bi, Andrew Poustie, Anthony J. Bednar, David J. Hanigan, Paul
861 Westerhoff, James F. Ranville, 2020. Quantifying temporal and geographic variation in
862 sunscreen and mineralogic titanium-containing nanoparticles in three recreational rivers,
863 Science of The Total Environment, Volume 743, 140845,
864 https://doi.org/10.1016/j.scitotenv.2020.140845.
865
866 43 Mueller, N.C., Nowack, B., 2008. Exposure modelling of engineered nanoparticles in
867 the environment. Environ. Sci. Technol. 42, 44447–53. https://doi.org/10.1021/es7029637
868

869 44 Silva, B.F. da, Pérez, S., Gardinalli, P., Singhal, R.K., Mozeto, A.A., Barceló, D., 2011.
870 Analytical chemistry of metallic nanoparticles in natural environments. TrAC - Trends Anal.
871 Chem. https://doi.org/10.1016/j.trac.2011.01.008
872
873 45 Wigginton, N.S., Haus, K.L., Hochella Jr, M.F., 2007. Aquatic environmental
874 nanoparticles. J. Environ. Monit. 9, 1306. https://doi.org/10.1039/b712709j
875
876 46 Panagosa, P., Borrellia, P., Poesen, J., Ballabioa, C., Lugatoa, E., Meusburger, K.,
877 Montanarella, L., Alewell, C. The new assessment of soil loss by water erosion in Europe.
878 Environmental Science & Policy Volume 54, December 2015, Pages 438-447.
879 https://doi.org/10.1016/j.envsci.2015.08.012
880
881 47 Choi, S., Johnston, M., Wang, G., Huang, C.P., 2018. A seasonal observation on the
882 distribution of engineered nanoparticles in municipal wastewater treatment systems
883 exemplified by TiO2 and ZnO. Science of the Total Environment 625, 1321-1329
884
885 48 Zhang, X., Wang, M., Guo, S., Zhang, Z., Li, H., 2017. Effects of weathering and rainfall
886 conditions on the release of SiO2, Ag, and TiO2 engineered nanoparticles from paints. J.
887 Nanopart. Res. 19, 338-347. https://doi.org/10.1007/s11051-017-4022-4
888
889 49 Azimzada, A., Farner, J. M., Hadioui, M., Liu-Kang, C., Jreije, I., Tufenkji, N., Wilkinson,
890 K. J., 2020. Relase of TiO2 nanoparticles from painted surfaces in cold cli-mates:
891 characterization using a high sensitivity single-particle ICP-MS. Environ. Sci.: Nano, 7, 139-148.
892 https://doi.org/10.1039/C9EN00951E

50 Hischier, R., Nowack, B., Gottschalk, F., Hincapie, I., Steinfeldt, M. & Som, C. Life cy-cle assessment of façade coating systems containing manufactured nanomaterials. J Nanopart Res 17, 68 (2015). https://doi.org/10.1007/s11051-015-2881-0

51 Neal, C., Jarvie, H., Rowland, P., Lawler, A., Sleep, D., Scholefield, P., 2011. Titanium in UK rural, agricultural and urban/industrial rivers: Geogenic and anthropogenic colloidal/sub-colloidal sources and the significance of within-river retention. Sci. Total Environ. 409, 1843–1853. https://doi.org/10.1016/j.scitotenv.2010.12.021

52 Greenwood, N.N., Earnshaw, A., 2012. Chemistry of the Elements. Elsevier.

53 Pradas del Real, A.E., Castillo-Michel, H., Kaegi, R., Larue, C., de Nolf, W., Reyes-Herrera, J., Tucoulou, R., Findling, N., Salas-Colera, E., Sarret, G., 2018. Searching for relevant criteria to distinguish natural vs. anthropogenic TiO 2 nanoparticles in soils. Environ. Sci. Nano. https://doi.org/10.1039/C8EN00386F

54 Goodall, P., Foulkes, M.E., Ebdon, L., 1993. Slurry nebulization inductively coupled plasma spectrometry-the fundamental parameters discussed. Spectrochim. Acta Part B At. Spectrosc. 48, 1563–1577. https://doi.org/10.1016/0584-8547(93)80143-I

55 Benedetti, M.F., Dia, A., Riotte, J., Chabaux, F., Gérard, M., Boulègue, J., Fritz, B., Chauvel, C., Bulourde, M., Déruelle, B., Ildefonse, P., 2003. Chemical weathering of basaltic

916 lava flows undergoing extreme climatic conditions: The water geochemistry record. Chem.
917 Geol. 201, 1–17. https://doi.org/10.1016/S0009-2541(03)00231-6
918
919 56 Xiao, C., Ye, J., Esteves, R. M., and Rong, C. (2016) Using Spearman's correlation
920 coefficients for exploratory data analysis on big dataset. Concurrency Computat.: Pract. Exper.,
921 28: 3866– 3878. doi: 10.1002/cpe.3745.
922
923 57 Domingos, R.F., Tufenkji, N., Wilkinson, K.J., 2009. Aggregation of titanium dioxide
924 nanoparticles: Role of a fulvic acid. Environ. Sci. Technol. 43, 1282–1286.
925 https://doi.org/10.1021/es8023594
926
927 58 Topuz, E., Sigg, L., Talinli, I., 2014. A systematic evaluation of agglomeration of Ag and
928 TiO_2 nanoparticles under freshwater relevant conditions. Environ. Pollut. 193, 37–44.
929 https://doi.org/10.1016/j.envpol.2014.05.029
930
931 59 Topuz, E., Talinli, I., 2015. Agglomeration of Ag and TiO_2 nanoparticles in surface and
932 wastewater: Role of calcium ions and of organic carbon fractions. Environ. Pollut. 204, 313–
933 323. https://doi.org/10.1016/j.envpol.2015.05.034
934
935 60 Chen, Y., Gao, Q., Chen, W., Wu, F., Yang, Y., Werner, D., Tao, S., Wang, X., 2018. A
936 mechanistic study of stable dispersion of titanium oxide nanoparticles by humic acid. Water
937 Res. 135, 85–94. https://doi.org/10.1016/j.watres.2018.02.018
938

939 61 Shih, Y. hsin, Zhuang, C. ming, Peng, Y.H., Lin, C. han, Tseng, Y. ming, 2012. The effect
940 of inorganic ions on the aggregation kinetics of lab-made TiO_2 nanoparticles in water. Sci. Total
941 Environ. 435–436, 446–452. https://doi.org/10.1016/j.scitotenv.2012.06.076
942
943 62 Zhang, Y., Chen, Y., Westerhoff, P., Crittenden, J., 2009. Impact of natural organic
944 matter and divalent cations on the stability of aqueous nanoparticles. Water Res. 43, 4249–
945 4257. https://doi.org/10.1016/j.watres.2009.06.005
946
947 63 French, R. A., Jacobson, A.R., Kim, B., Isley, S.L., Penn, R.L.E.E., Baveye, P.C., 2009.
948 Influence of ionic strength, pH, and cation valence on aggregation kinetics of titanium dioxide
949 nanoparticles. Environ. Sci. Technol. 43, 1354–1359. https://doi.org/10.1021/es802628n
950
951 64 Ilina, S.M., Lapitskiy, S.A., Alekhin, Y. V., Viers, J., Benedetti, M., Pokrovsky, O.S., 2016.
952 Speciation, Size Fractionation and Transport of Trace Elements in the Continuum Soil Water–
953 Mire–Humic Lake–River–Large Oligotrophic Lake of a Subarctic Watershed. Aquat.
954 Geochemistry 22, 65–95. https://doi.org/10.1007/s10498-015-9277-8
955
956 65 Praetorius, A., Labille, J., Scheringer, M., Thill, A., Hungerbühler, K., Bottero, J.Y., 2014.
957 Heteroaggregation of titanium dioxide nanoparticles with model natural colloids under
958 environmentally relevant conditions. Environ. Sci. Technol. 48, 10690–10698.
959 https://doi.org/10.1021/es501655v
960

961 66 Labille, J., Harns, C., Bottero, J.Y., Brant, J., 2015. Heteroaggregation of titanium dioxide
962 nanoparticles with natural clay colloids. Environ. Sci. Technol. 49, 6608–6616.
963 https://doi.org/10.1021/acs.est.5b00357
964
965 67 Wang, H., Adeleye, A.S., Huang, Y., Li, F., Keller, A.A., 2015. Heteroaggregation of
966 nanoparticles with biocolloids and geocolloids. Adv. Colloid Interface Sci. 226, 24–36.
967 https://doi.org/10.1016/j.cis.2015.07.002
968
969 68 Le Cloarec, M.F., Bonte, P.H., Lestel, L., Lefèvre, I., Ayrault, S., 2011. Sedimentary
970 record of metal contamination in the Seine River during the last century. Phys. Chem. Earth
971 36, 515–529. https://doi.org/10.1016/j.pce.2009.02.003
972
973 69 Pons-Branchu, E., Ayrault, S., Roy-Barman, M., Bordier, L., Borst, W., Branchu, P.,
974 Douville, E., Dumont, E., 2015. Three centuries of heavy metal pollution in Paris (France)
975 recorded by urban speleothems. Sci. Total Environ. 518–519, 86–96.
976 https://doi.org/10.1016/j.scitotenv.2015.02.071
977
978 70 Le Pape, P., Ayrault, S., Quantin, C., 2012. Trace element behavior and partition versus
979 urbanization gradient in an urban river (Orge River, France). J. Hydrol. 472–473, 99–110.
980 https://doi.org/10.1016/j.jhydrol.2012.09.042
981
982 71 Meybeck, M., Lestel, L., Bonté, P., Moilleron, R., Colin, J.L., Rousselot, O., Hervé, D., de
983 Pontevès, C., Grosbois, C., Thévenot, D.R., 2007. Historical perspective of heavy metals
984 contamination (Cd, Cr, Cu, Hg, Pb, Zn) in the Seine River basin (France) following a DPSIR

approach (1950-2005). Sci. Total Environ. 375, 204–231. https://doi.org/10.1016/j.scitotenv.2006.12.017

72 Viers, J., Dupré, B., Gaillardet, J., 2009. Chemical composition of suspended sediments in World Rivers: New insights from a new database. Sci. Total Environ. 407, 853–868. https://doi.org/10.1016/j.scitotenv.2008.09.053

73 Chen, J. Bin, Gaillardet, J., Bouchez, J., Louvat, P., Wang, Y.N., 2014. Anthropophile elements in river sediments: Overview from the Seine River, France. Geochemistry, Geophys. Geosystems 15, 4526–4546. https://doi.org/10.1002/2014GC005516

74 Barbieri M, 2014 The Importance of Enrichment Factor (EF) and Geoaccumulation Index (Igeo) to Evaluate the Soil Contamination. J Geol Geophys 2016, 5:1 ,https://doi.org /10.4172/2381-8719.1000237

75 Besold J., Kumar N., Scheinost A. C., Lezama Pacheco J., Fendorf S., and Planer-Friedrich B. Environmental Science & Technology 2019 53 (9), 5005-5015

76 Biswas A., Besold J., Sjöstedt C., Gustafsson J., Scheinost A. C. and Planer-Friedrich B. Environmental Science & Technology 2019 53 (18), 10723-10731
DOI: 10.1021/acs.est.9b03020

77 Besold J., Eberle A., Noël V., Kujala K., Kumar N., Scheinost A. C., Lezama Pacheco J., Fendorf S., and Planer-Friedrich B. Environmental Science & Technology 2019 53 (18), 10792-10802 DOI: 10.1021/acs.est.9b03924

78 Sharma, B., Sarkar, A., Singh, P., Singh, R.P., 2017. Agricultural utilization of biosolids: A review on potential effects on soil and plant grown. Waste Manag. 64, 117–132. https://doi.org/10.1016/j.wasman.2017.03.002

Table 1: Experimental conditions of sp-ICPMS measurement.

Table 2: Average (range) of some physicochemical properties of three catchment waters. Original data taken from *Wang et al. (2020) (Table S2 in supplementary information [25])*.

Table 3: Concentrations of NPs-TiO_2 measured in surface water from the literature and this study. n.g.: not given. n.a.: not analysed. *Ti: total content of filtered fraction after digestion. ** Engineered nanoparticles only as defined in [24].

Table 4: Average enrichment factor (EF) of selected elements in three small catchments normalized to suspended matter particles (SRSM) of Seine River.

Fig. 1: Sampling location and their land-use. Blue arrows indicate the direction of the water flow. Coloured boxes report the area of the watershed, the average population density (Pop. Dens.) and measured annual average water flow rate ($L.sec^{-1}$) for each watershed.

Figure 2: Particle number concentration (PNC) of NPs-TiO2 measured at the three sites during one-year of sampling. Samples were taken once per month, except for three months which are missing.

Figure 3: Ti distribution (%) of total Ti for two fractions i.e., the ***NPs-TiO_2*** fraction (Ti-NPs) and large particles (Ti-Par) in three waters for one-year sampling, in which Ti-Par = Ti total – Ti NPs – Ti dissolved with Ti dissolved less than 1% of tot. Panel A, B and C showing the data of the forested, agricultural and urban watersheds, respectively. The numbers inserted in each bar correspond to the mass concentration given in µgTi L^{-1} of measured Ti-NPs and calculated Ti-Par.

Figure 4: Calculated diameters of the TiO_2-NPs detected by sp-ICPMS and comparison with recently published data (see supplementary section for detailed size calculation procedure). [21]: Donovan et al., 2016; [26]: Wu et al., 2020; [42]: Rand et al., 2020.

Figure 5: Left: SEM images of filters retaining suspended particles containing TiO_2, with different shapes, present in sampled waters. Panels (a) and (c) showing a sample from the forested and urban watersheds, respectively. Right: Panel (b) and (d) showing the EDX analysis of corresponding particles highlighted by the green circle in panel (a) and the green square in panel (c).

Figure 6: Particle number concentration (PNC) of NPs-TiO_2 as function of that of Ag NPs in agricultural and forested watersheds. Ag-NPs concentrations are from [25]. The correlation coefficients r corresponding to Agricultural orange and Forested green broken lines are equal to $r_{Agricultural}$ = 0.96 and $r_{forested}$ = 0.89. Their corresponding *p* value are equal to 0.00003 and 0.0004 for a sampling size n=9 and 10, respectively.

Figure 7: Mass concentration of NPs-TiO_2 as function of DOC concentration in water samples from the forested watershed. The correlation coefficient r corresponding to the orange broken line is equal to *r* = 0.91 and it corresponds to a *p* value equal to 0.0002 and a sampling size n=9

Figure 8: Mass concentration of TiO_2 NPs as function as that (bulk minus dissolved) of (a) Sb and (b) Ni in forested water. The correlation coefficients r corresponding to the orange broken line are equal to *r* = 0.91 and *r* = 0.89 in panel (a) and (b), respectively. They correspond to a *p* value equal to 0.0002 and 0.0005 with a sampling size n=10.

Figure 9: Export-rate of (a) nanoparticulate (b) dissolved < 1 kDa (c) total Ti detected in three waters along the sampling year.

Figure 1

Click here to access/download;Figure;Figure 1.tif

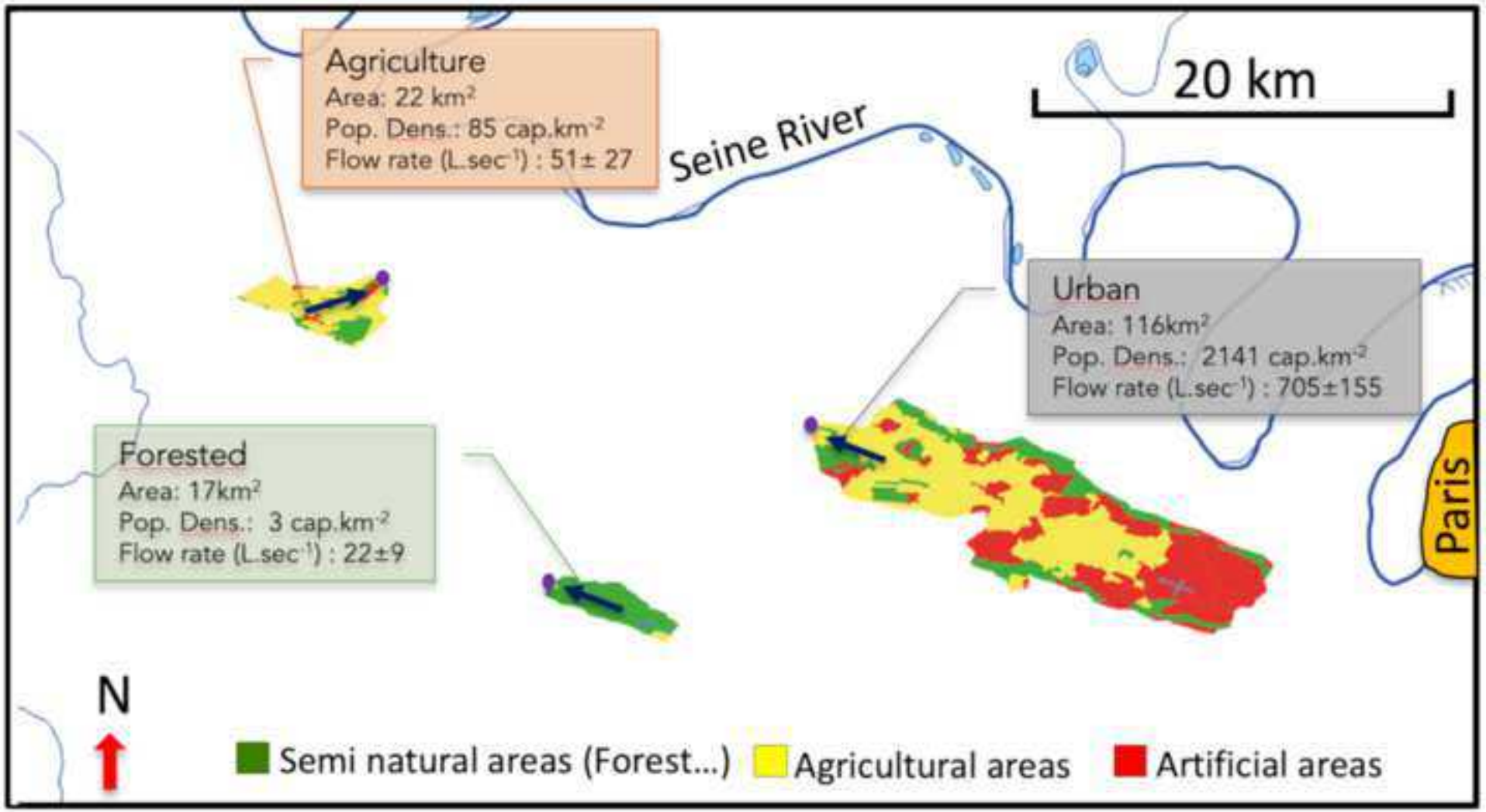

Figure 2

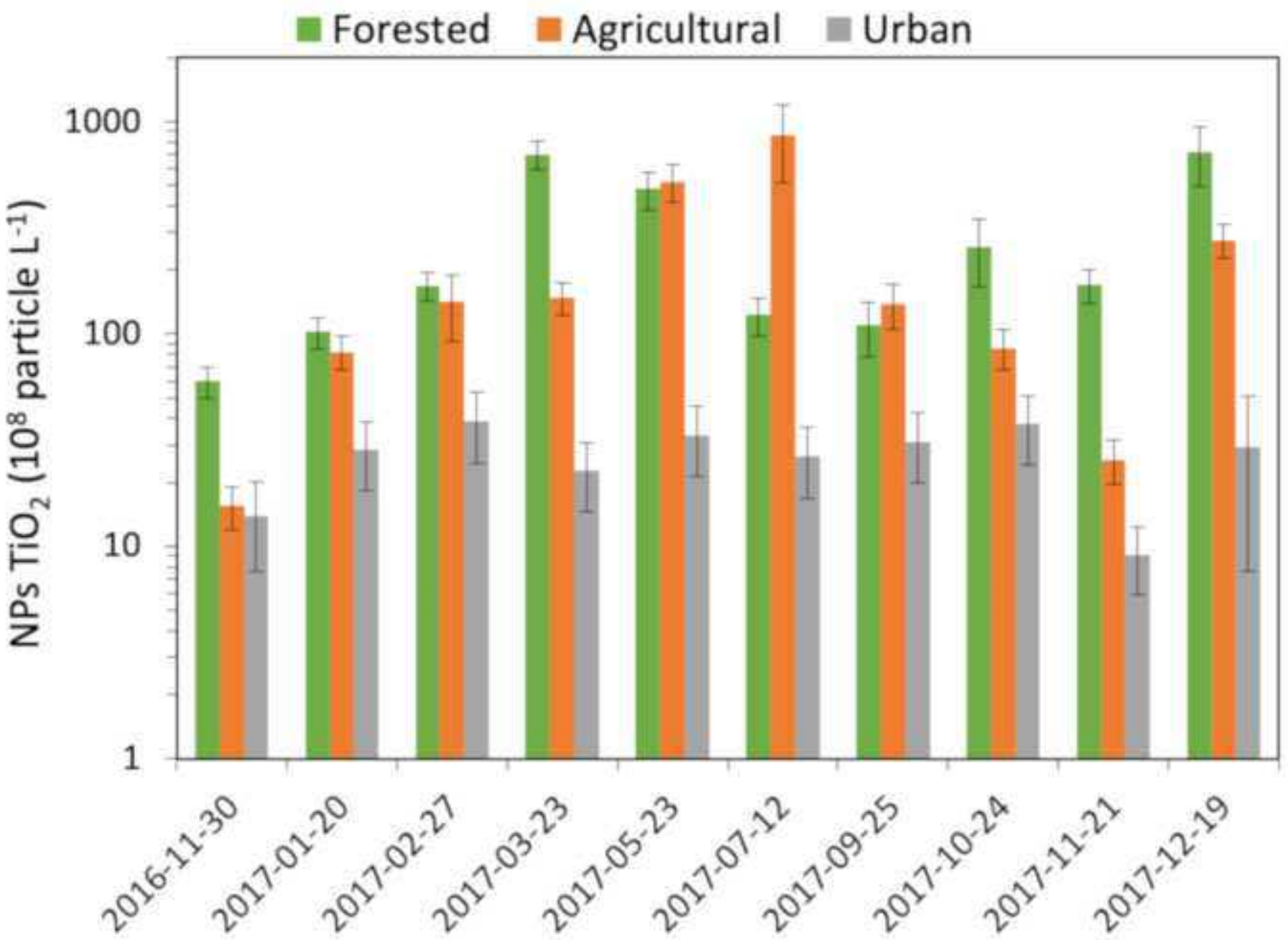

Figure 3 A

Click here to access/download;Figure;Figure 3 panel A.tif

Figure 3 B

Click here to access/download;Figure;Figure 3 panel B.tif

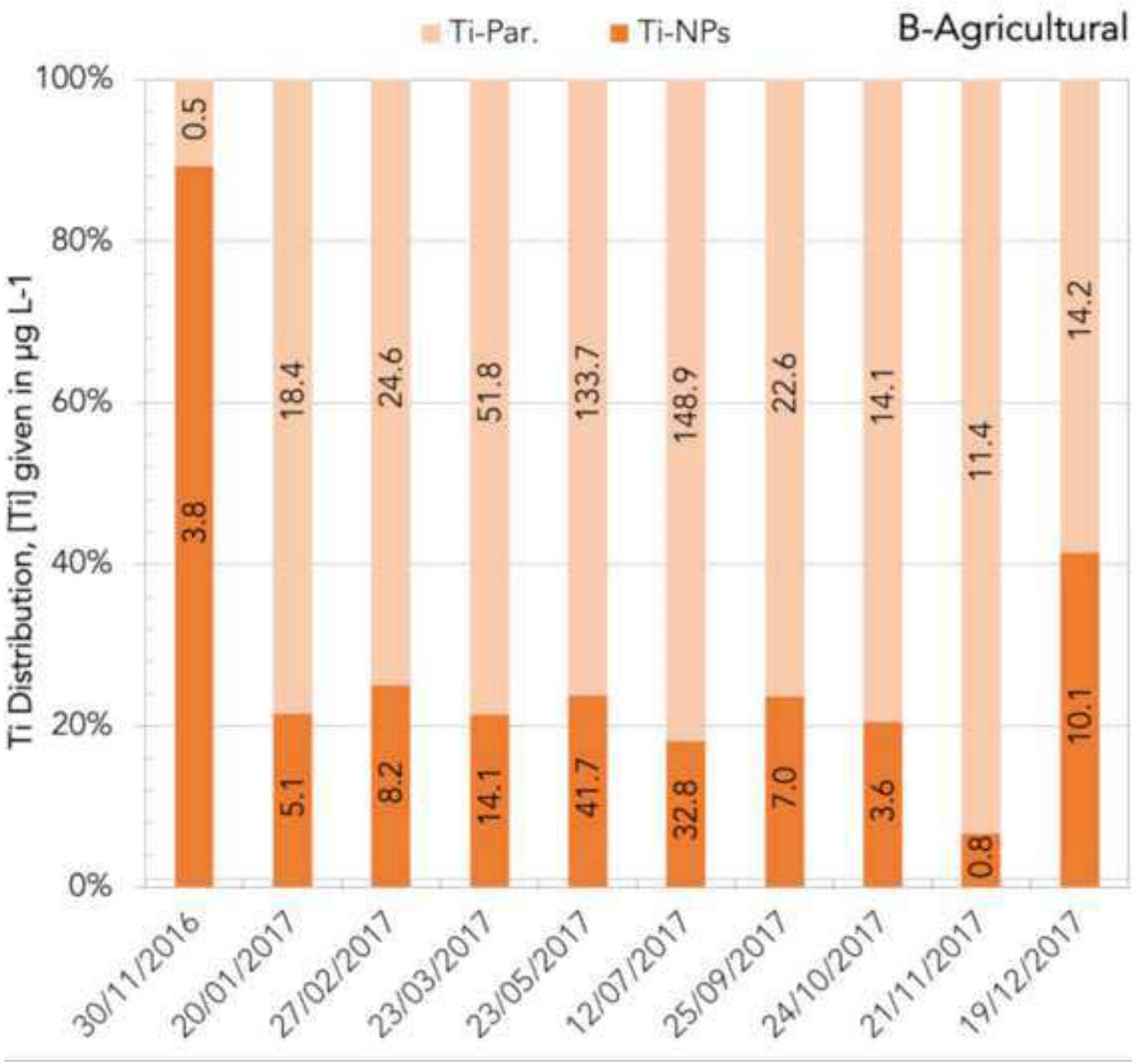

Figure 3 C

Click here to access/download;Figure;Figure 3 panel C.tif

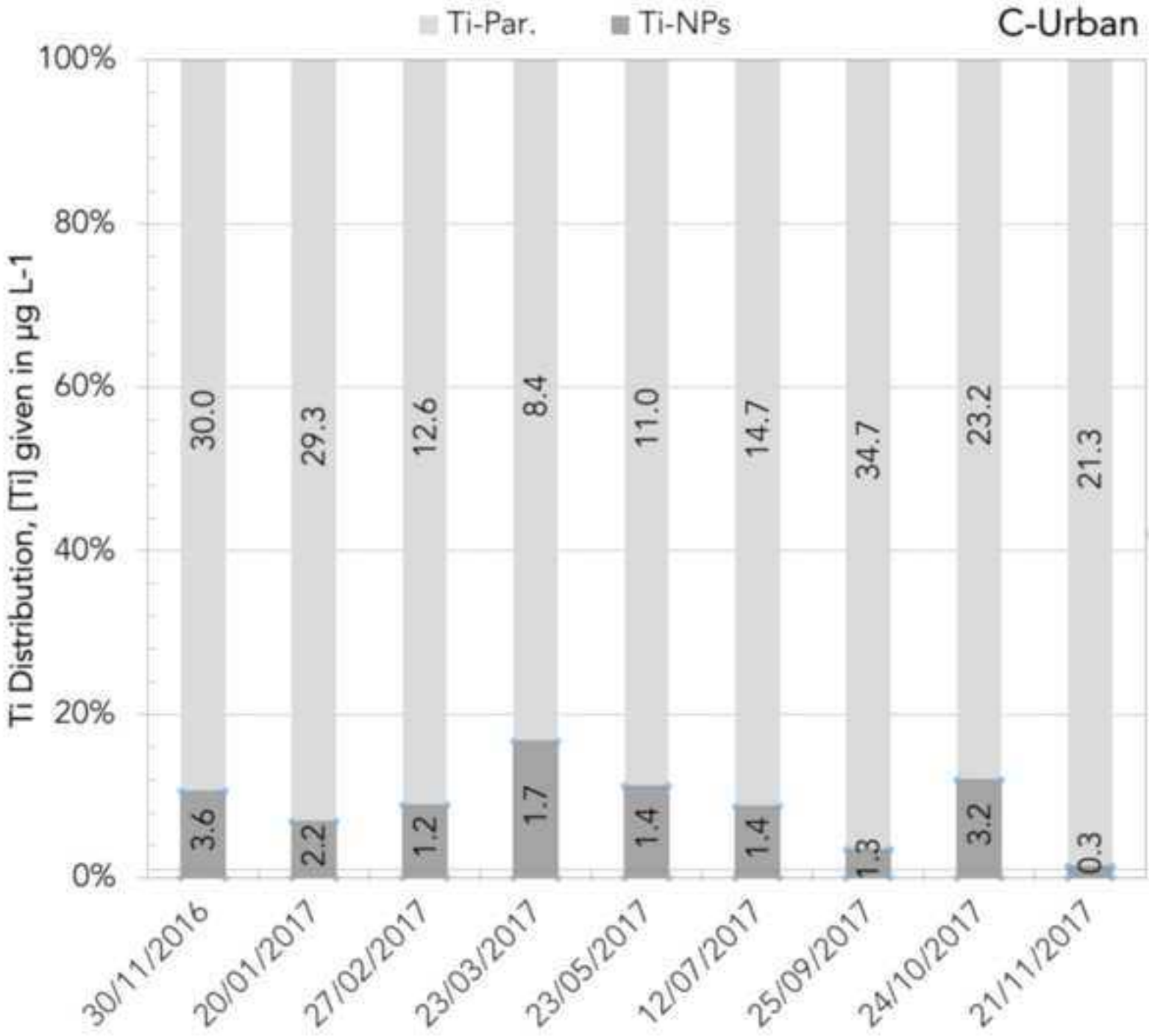

Figure

Click here to access/download;Figure;Figure 4.tif

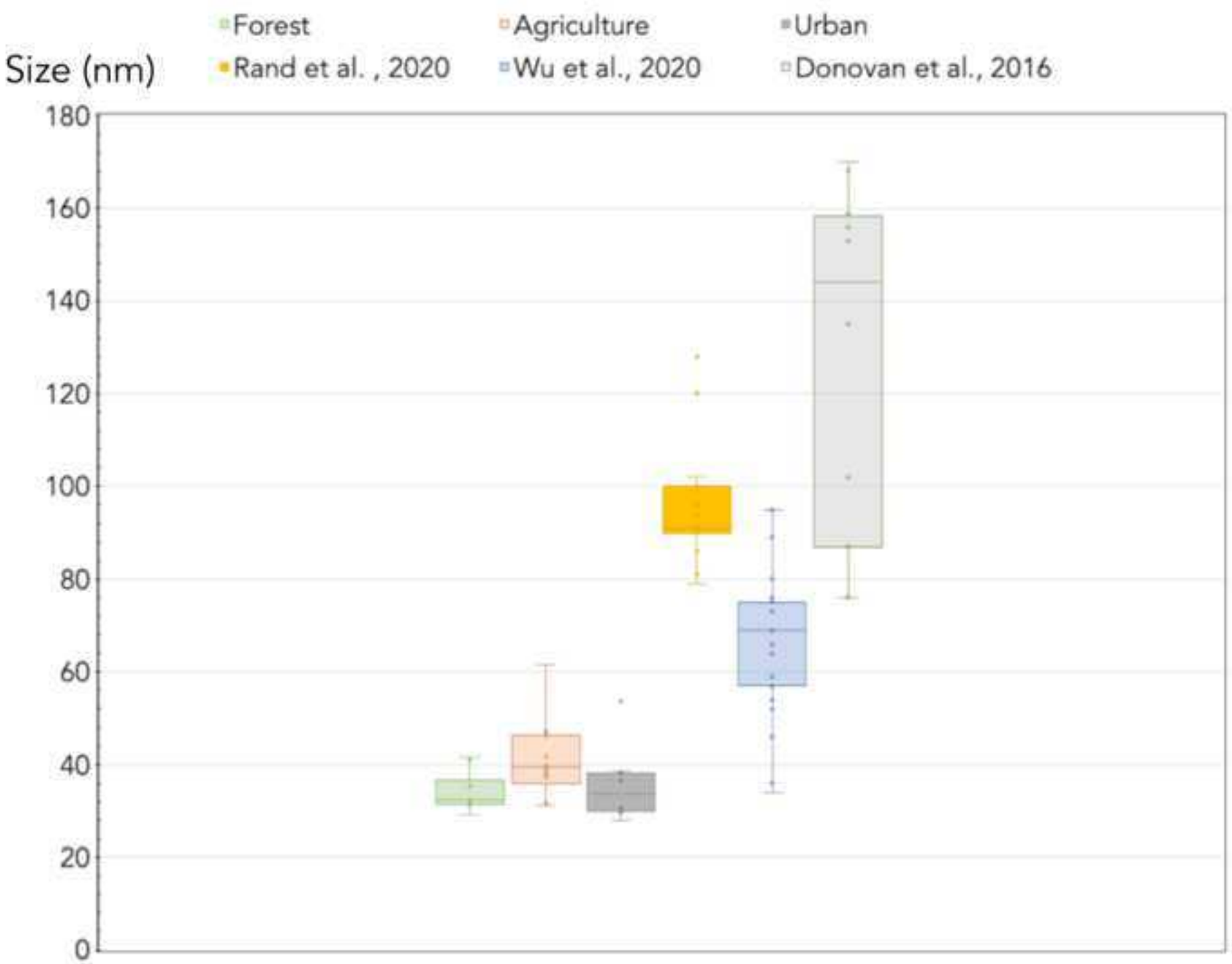

Figure 5 A-B

Click here to access/download;Figure;Figure 5 panel a b.tif

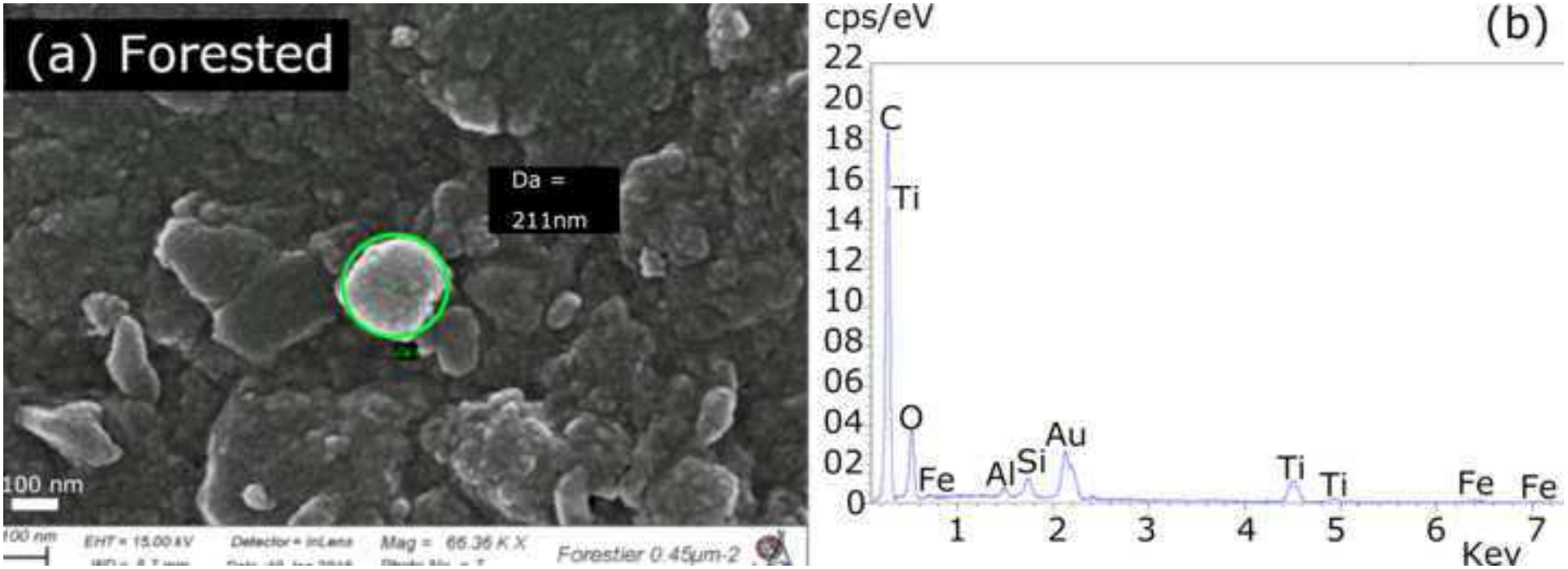

text1200.png

Figure 5 C-D

Click here to access/download;Figure;Figure 5 panel c d.tif

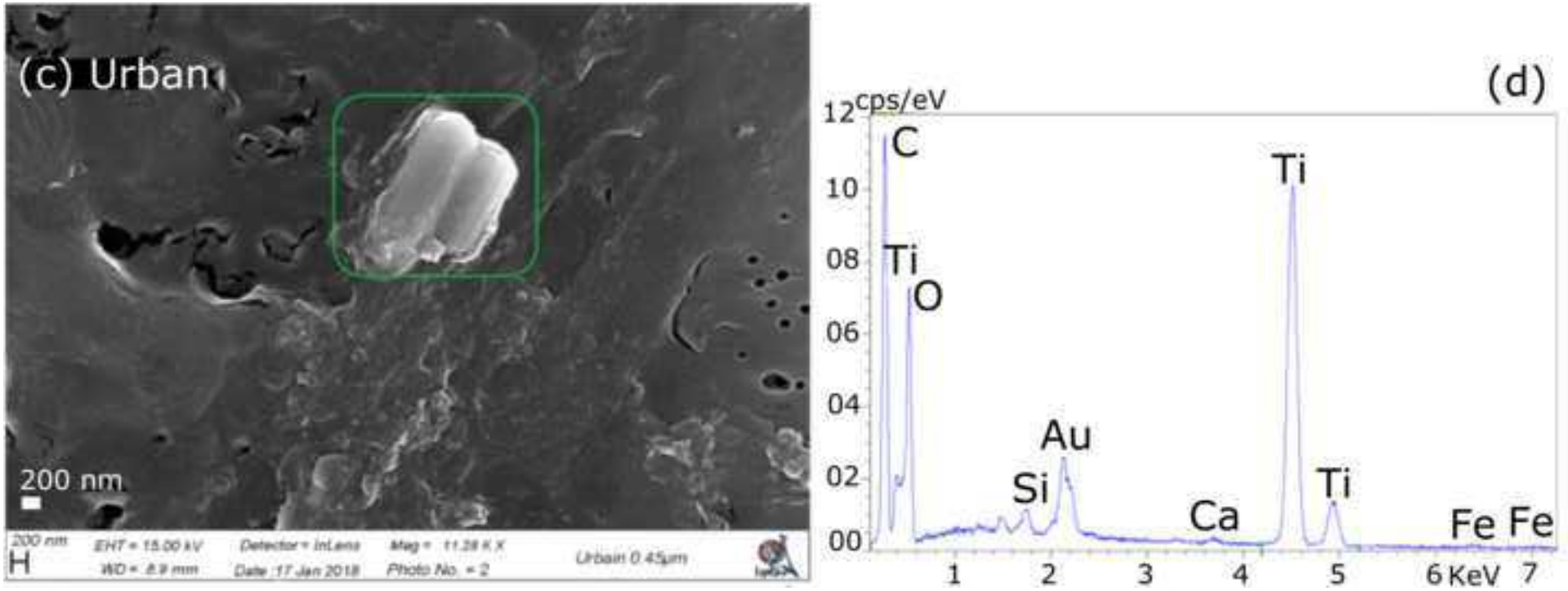

image.png

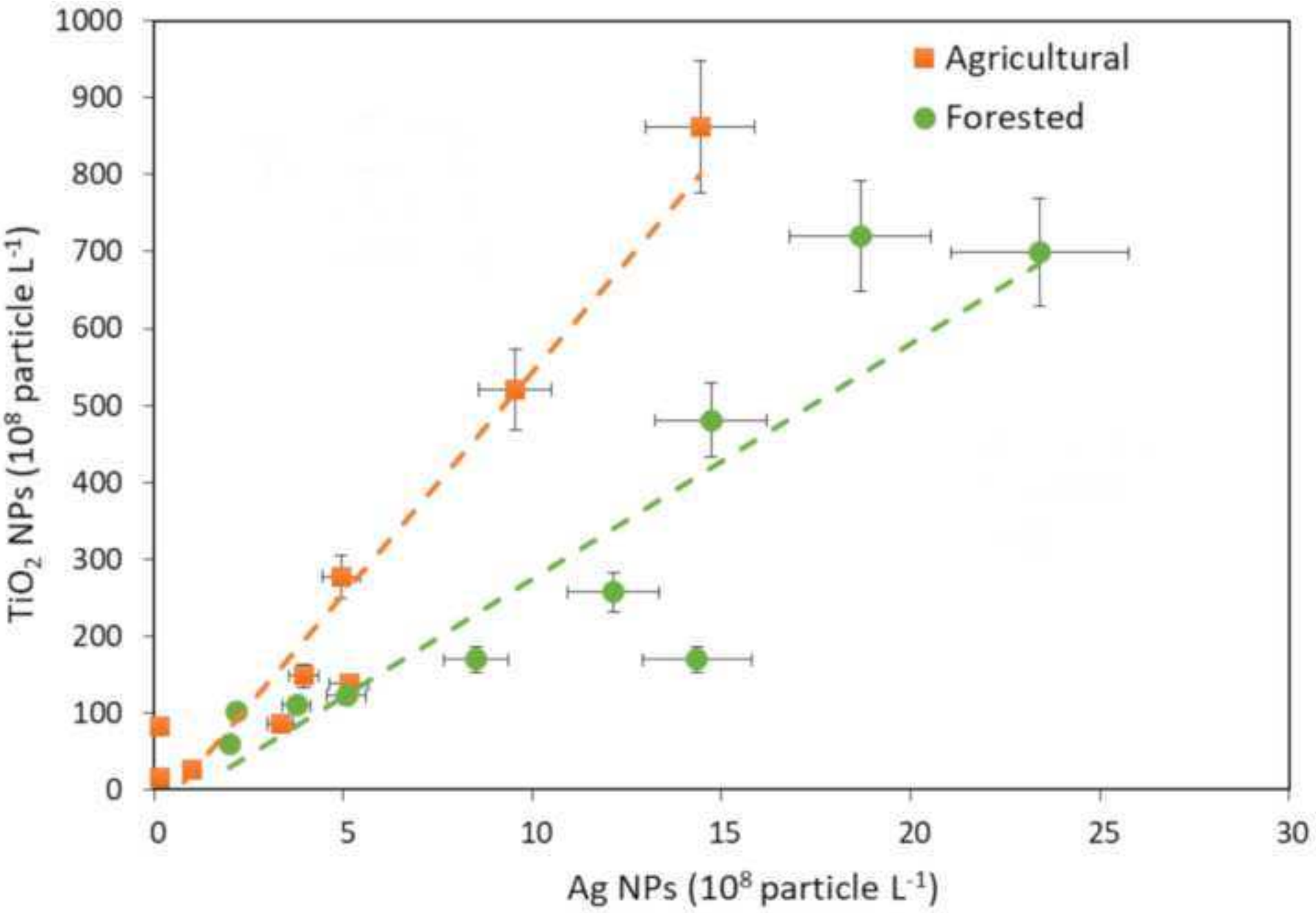

Figure 6.tif

Figure 7

Click here to access/download;Figure;Figure 7.tif

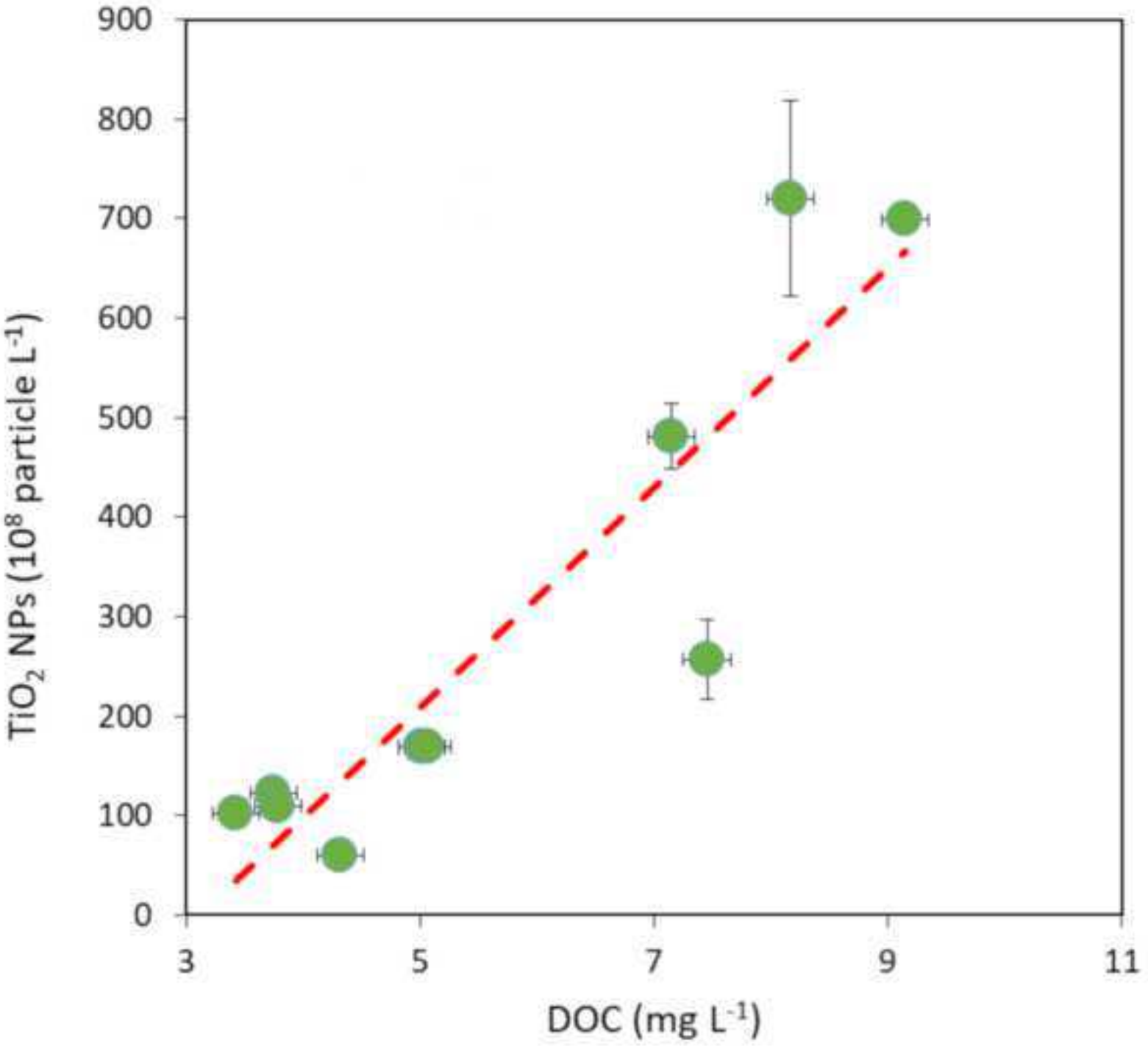

Figure 7.tif

Figure 8 A

Click here to access/download;Figure;Figure 8 panel a.tif

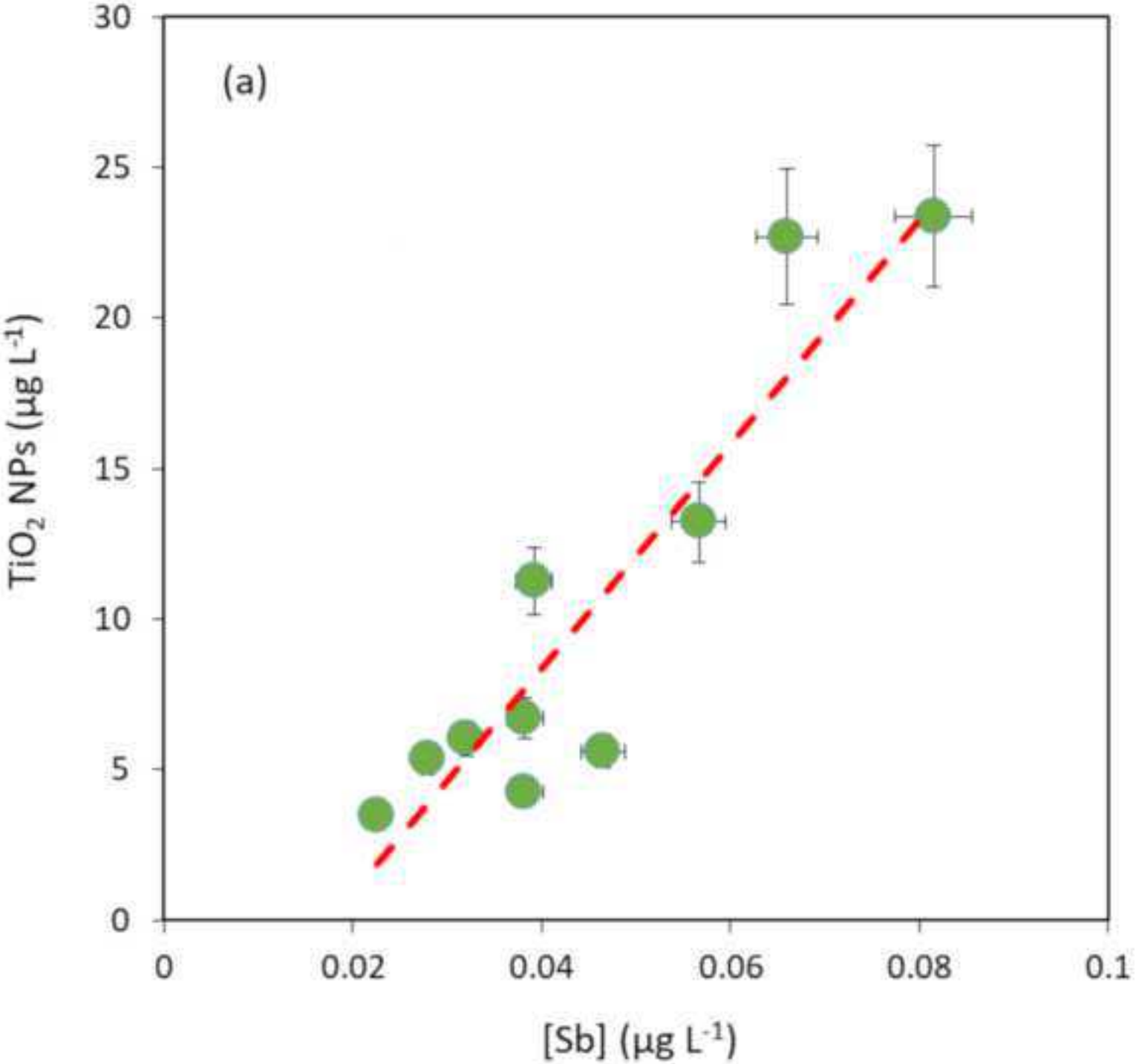

Figure 8 panel a.tif

Figure 8 B

Click here to access/download;Figure;figure 8 panel b.tif

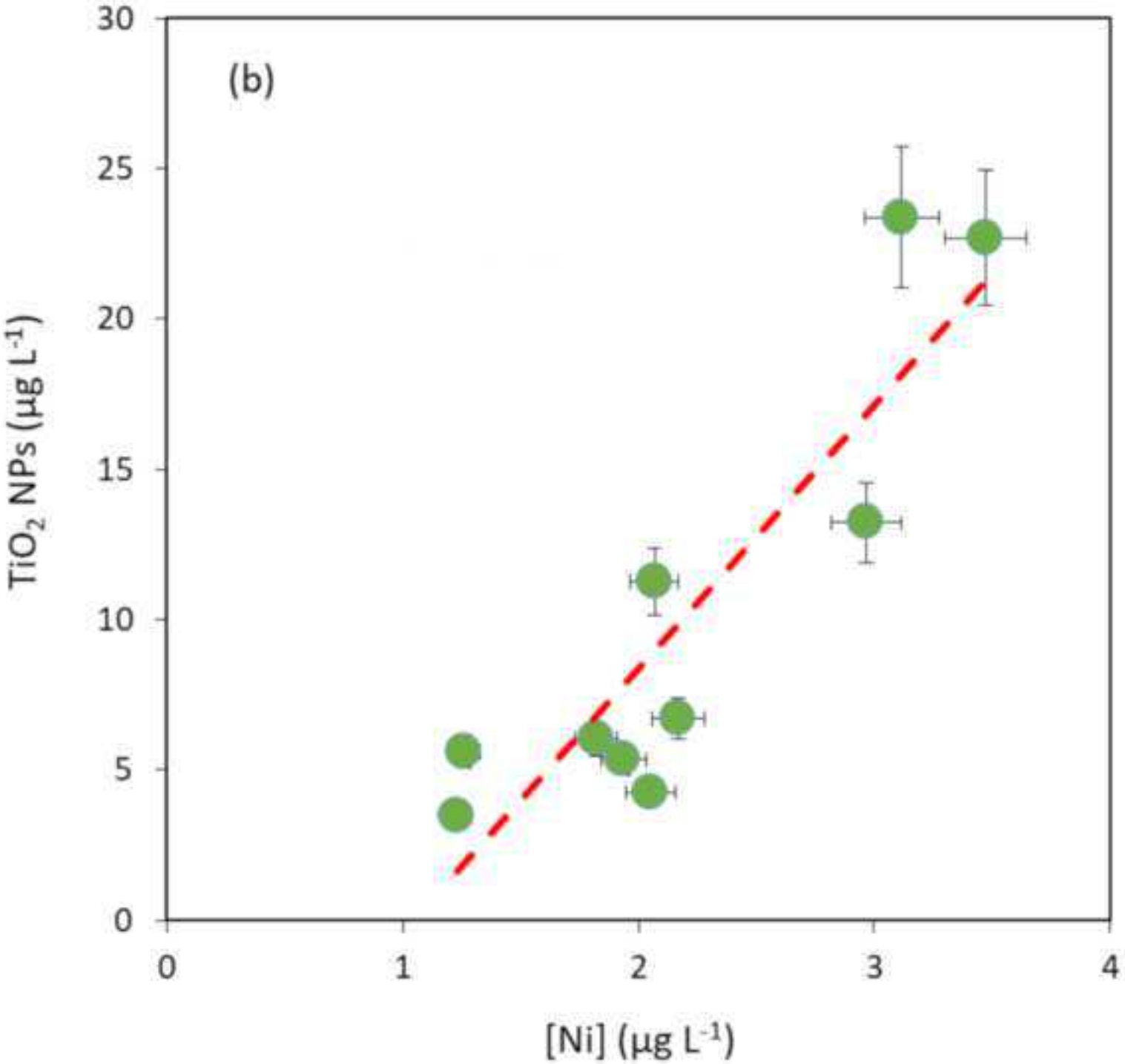

figure 8 panel b.tif

Figure 9 A

Click here to access/download;Figure;Figure 9 panel a.tif

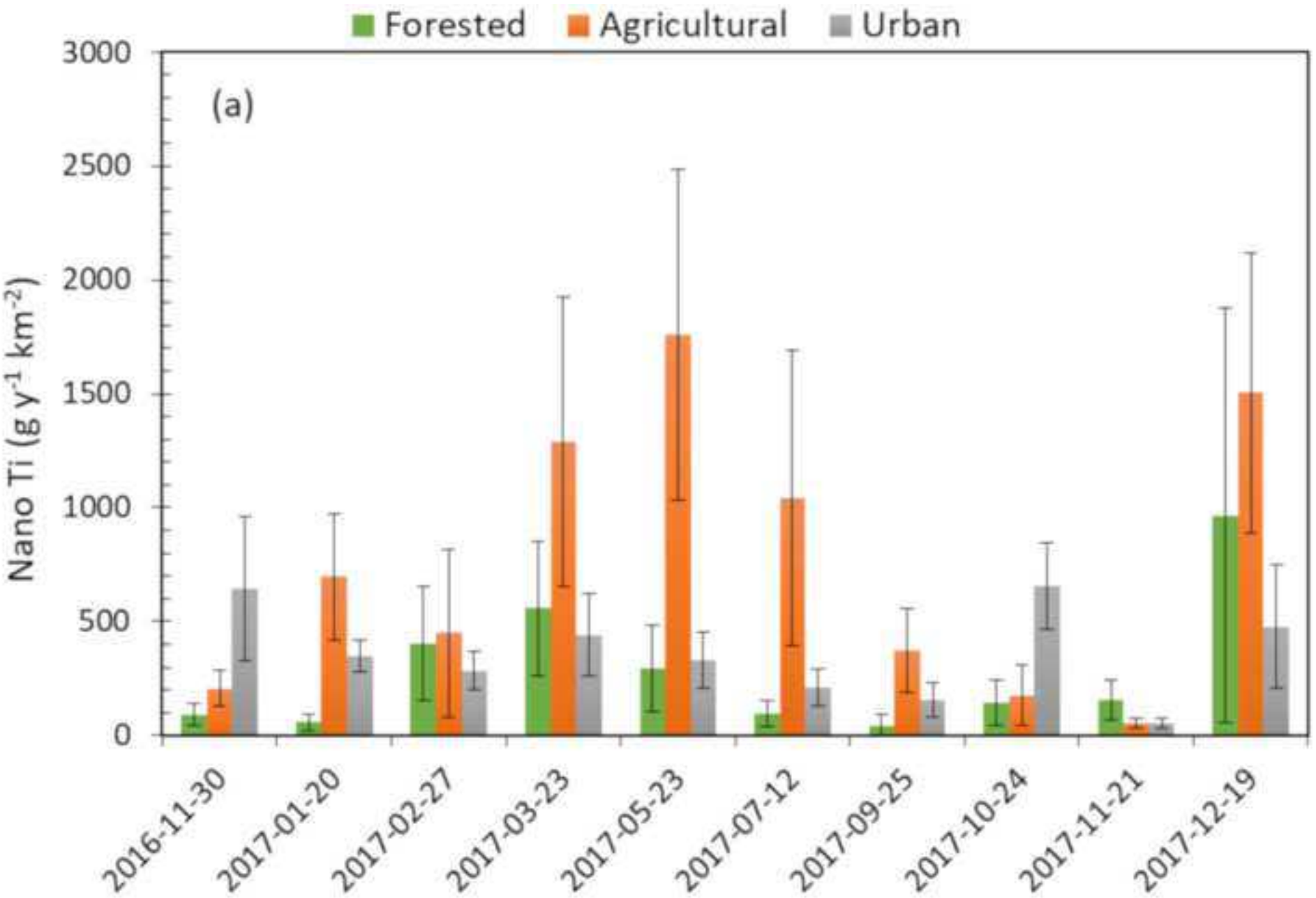

Figure 9 B

Click here to access/download;Figure;Figure 9 panel b.tif

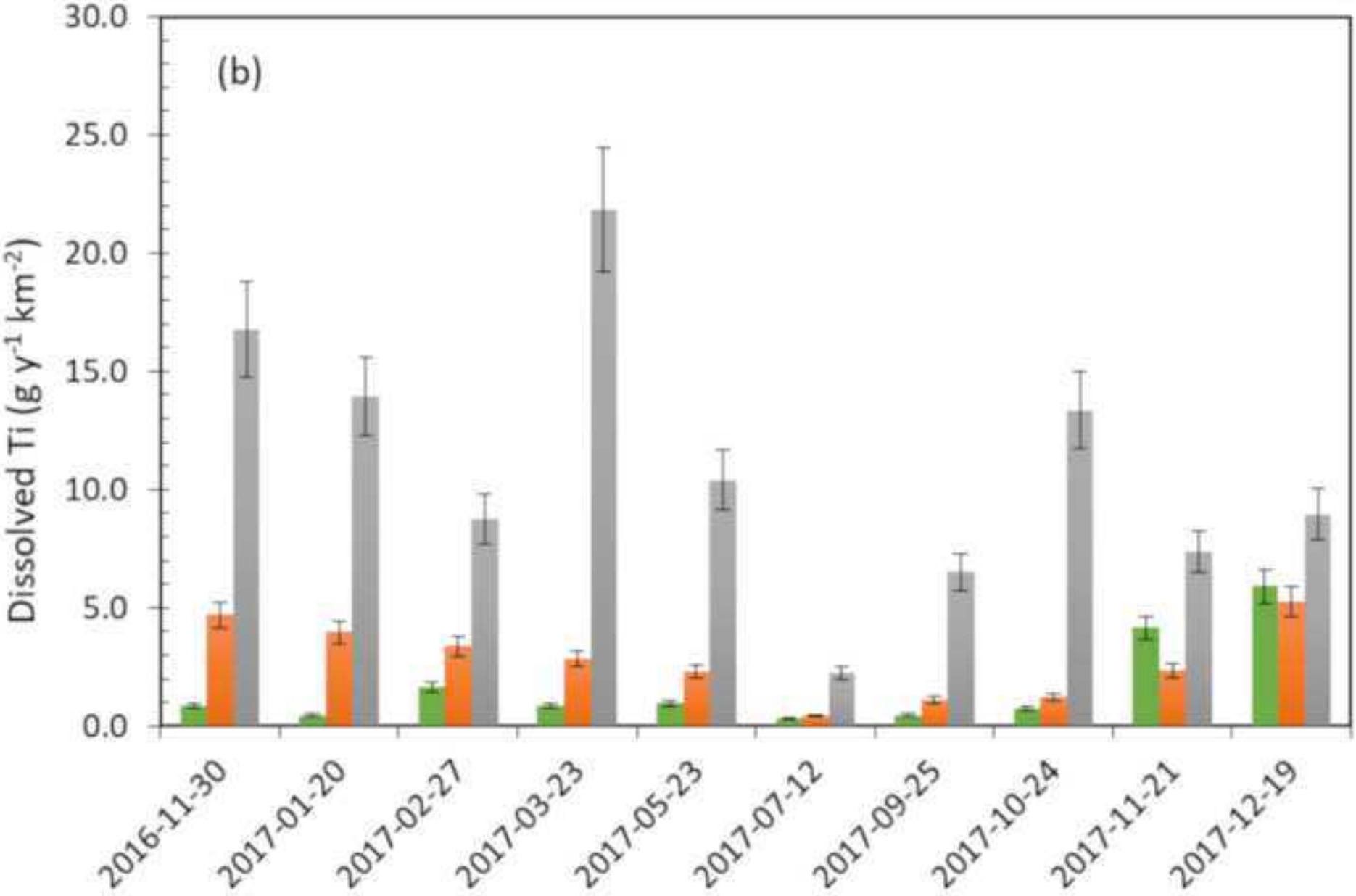

Figure 9 C

Click here to access/download;Figure;Figure 9 panel c.tif

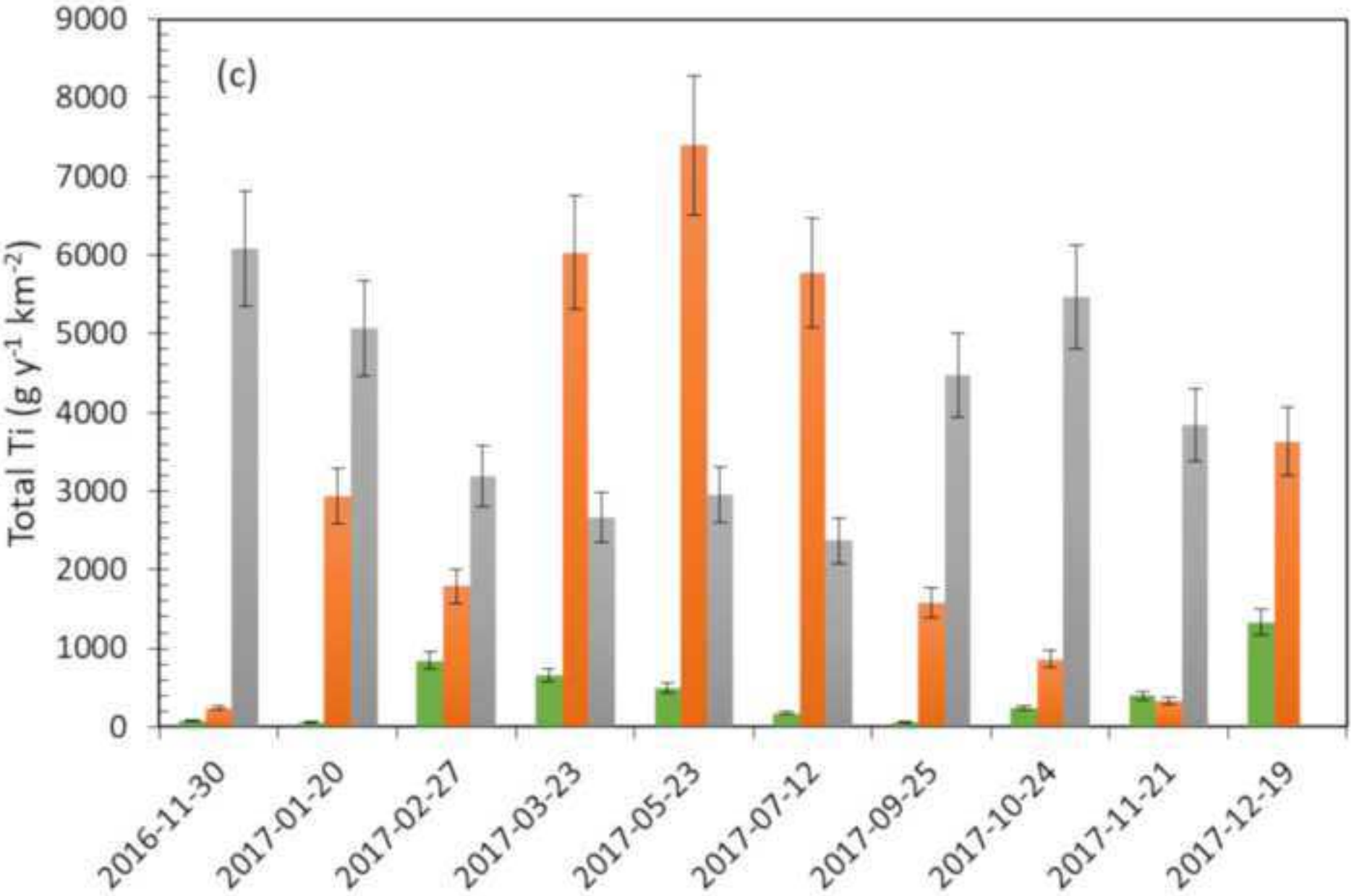

Titanium nanoparticles fate in small-sized watersheds under different land-uses

Additional Informations

Jia-Lan Wang[1, 2], Enrica Alasonati[2], Paola Fisicaro[2], Marc F. Benedetti[1]*

[1] Université de Paris, Institut de physique du globe de Paris, CNRS, UMR 7154, F-75238 Paris, France

[2] Department of Biomedical and Inorganic Chemistry, Laboratoire National de Métrologie et d'Essais (LNE), 1 rue Gaston Boissier, Paris, 75015 France

*Corresponding author
Email: benedetti@ipgp.fr (M. F. Benedetti)
Phone number: +33 1 83 95 76 95

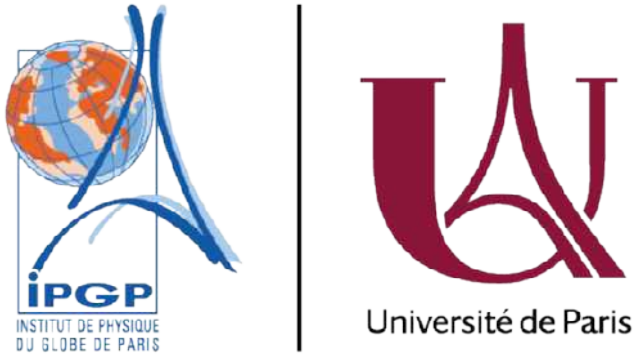

***Table S1**: Characteristics of three small watersheds of the Seine River.*

	Watershed	**Forested**	**Agricultural**	**Urban**
	City	Gambaiseuil	Monchauvet	Beynes
	Area (km^2)	17	22	116
	River	Ponts Quentin	Vaucouleurs	Gally
	Latitude	48.7575	48.885736	48.870527
	Longitude	1.735392	1.624297	1.889618
	(*)Flow rate (m^3/s)	0.02	0.05	0.70
Land use	Forestry	95%	22%	19%
	Agriculture	5%	72%	44%
	Artificial areas		6%	37%
Lithology	Limestone		67%	63%
	Chalk			20%
	Sand	100%	33%	17%

(*)annual average

***Table S2**: Digestion efficiency of two commercial standards of TiO_2 NPs (Aerodisp and P25) in Milli Q and Evian waters.*

	TiO_2 (µg L^{-1})	Matrix	Recovery (%)
Aerodisp	20	MQ	115
Aerodisp	100	MQ	102
Aerodisp	400	MQ	105
P25	8000	MQ	111
P25	15000	Evian	95
P25	32000	MQ	111
P25	40000	MQ	102

Quantification of TiO_2 particle number concentration (PNC) by single particle ICPMS (sp-ICPMS)

1. Subtraction approach used for sp-ICPMS data analysis

The ultra-filtrate (< 1 kDa) of sampled water represents well the matrix environment and thus its signal was used as the blank of TiO_2 NPs present in sampled waters. Blanks have been prepared for each sampled water because the water chemistry varied from one site or one sample period to another. First, spectrums of intensity *versus* time for water sample and the corresponding ultra-filtered blank (Figure S1) were converted into the histograms of frequency *versus* intensity. Then, the frequency of the blank was subtracted from that of the unknown sample of the same matrix at the same intensity interval. This subtracted frequency was used to calculate the particle number concentration. The methodology validation is presented in the following section.

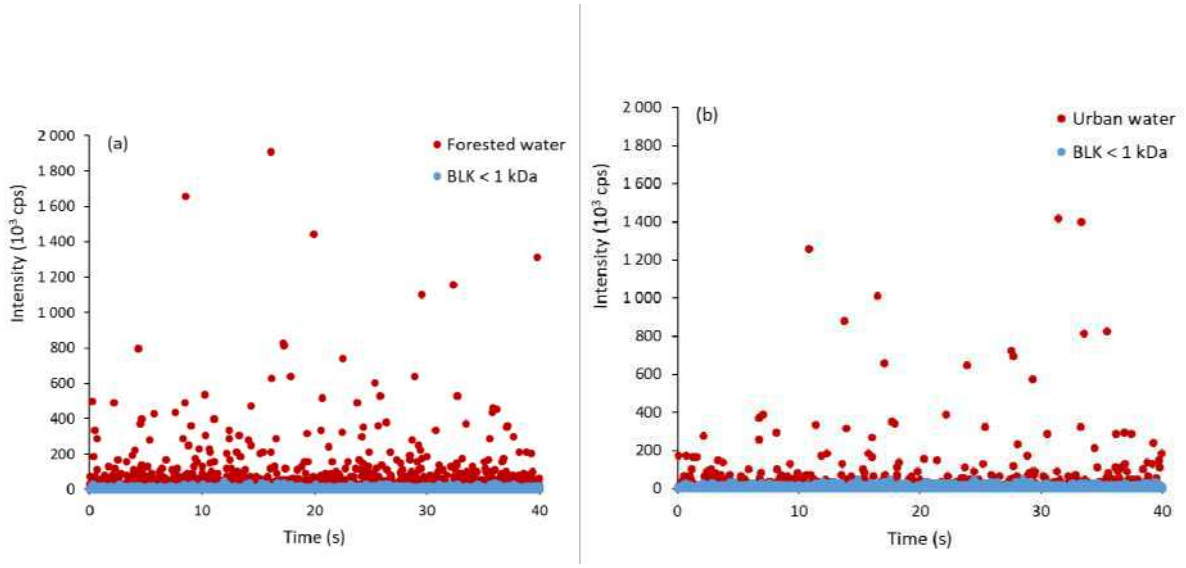

***Figure S1**: ^{47}Ti signal intensity of river samples and their blank (ultra-filtrate < 1 kDa) as function of the time for (a) forested and (b) urban watersheds.*

2. Methodology validation

2.1 Calculation of transport efficiency (η)

In the spray chamber, more than 90% of sample is redirected into waste and only a small fraction is transported into plasma, leading to differences in mass delivery. This transport loss of sample is termed as "transport efficiency" (η), an essential factor required to calculate the concentration and size of NPs. In the present study, the method referred to as the particle size method [S1] was applied to calculate η since the applied reference material (Au-NPs) is certified for the particle size other than the concentration.

Given that transport efficiencies and sensitivity of particulate and dissolved standards are the same, η is the ratio of the slope of calibration curve of Au-NPs (R_{NP}, cps g^{-1}) to that of corresponding dissolved Au^{3+} (R_{diss}, cps g^{-1}). R_{NP} can be directly calculated from the mass (m_{NP}, g) of one Au-NP with certified size and the corresponding ICPMS response (I_{NP}, cps). While, R_{diss} equals to the response of dissolved ions calibration (RF_{ion}, cps g^{-1} L^{-1}) divided by the uptake flow (q_{liq}, L s^{-1}) and the dwell time (t_d, s):

$$\eta = \frac{R_{diss}}{R_{NP}} = \frac{RF_{ion} \times m_{NP}}{I_{NP} \times q_{liq} \times t_d} \quad (1)$$

The standard suspension is certified for the size (55.4 nm in average) and the mass concentration of Au is given as 51.86 µg mL^{-1}. Given that all Au is in form of nanoparticles of 55.4 nm and Au-NPs are spherical, the particle number concentration can be calculated (3.0 x 10^{10} particle mL^{-1}). Usually, the stock suspension is diluted 2.5 x 10^5 times to avoid NPs coincidence at very short dwell time. The suspension used to evaluate η is at the concentration of 2.1 x 10^{-4} µg ml^{-1} (1.2 x 10^5 particle mL^{-1}). Transport efficiency has been evaluated for each sampling mission and the average value was equal to 9% ± 2%.

2.2 Experiments performed to confirm the methodology

To confirm the methodology, three samples have been spiked with the smallest standards of NPs commercially available, the gold colloidal solutions of 10 nm (BBI, batch 026677). Certified nanoparticles of smaller size do not exist for TiO_2, Au and Ag to the best of our knowledge. The ultrafiltration step was conducted the same day than sample collection to avoid any preparation artefacts. Samples have been prepared as follows:

1. Sample from the forest site (sample 19/12/2017) doped with Au NPs of 10 nm.
2. Ultrafiltered fraction of the forest site sample (19/12/2017), doped with Au NPs of 10 nm.

3. MQ water doped with Au NPs of 10 nm.

These experiments allowed to determine the ultrafiltration efficiency to remove nanoparticles with our methodology. They also allowed to evaluate whether the calculated NPs sizes in the three media were within the range of the certified one (i.e. 10 nm) and to evaluate the detection limits. All samples were prepared and analysed the same day by HR-ICPMS in single particle mode. HR-ICPMS in the single particle mode conditions are similar to the one used for the data acquisition and described in the present paper. The gold calibration curve was in the range 0 to 1 µg L^{-1} in 1% HCl solutions. The transport efficiency was 9.1%, and was calculated as previously described.

Results are presented in Figures S2 to S4:

- Grey dots correspond to MQ water (MQ-D), the ultrafiltered water from the forested site sample treated the 19/5/2017 (UF-D) and the raw water from the same forested site sampled the same day (19/5/2017) (Raw-D) doped with the 10 nm certified gold solution.
- Orange dots correspond to the same samples but after an ultrafiltration at 1kD (MQ-D < 1KD, UF-D< 1KD, Raw-D < 1KD), conducted for all field water samples.
- Green dots correspond to the Au^{197} signal in MQ water acquired in low-resolution mode with HR-ICPMS in single particle mode.

***Table S3**: Summarizing the experiments performed to confirm the methodology and colour code of the data presented in figure S2 to S4.*

	MQ-D	UF-D	Raw-D	MQ-D<1KD	UF-D<1KD	Raw-D<1KD	MQ
Figure S2							
Figure S3							
Figure S4							

In addition, in each of the three figures a line has been added corresponding to 3 times the standard deviation of all values recorded for:

- the MQ< 1kD (blue line)
- the fraction < 1KD for samples UF-D<1KD (red line)
- Raw-D<1KD (red line).

Figures S2, S3 and S4 clearly show that most of the particles were removed by the ultrafiltration process at 1kD. The % of removal was calculated to be 94 ± 5%, 95 ± 5% and 93 % ± 5% for the Raw-D, UF-D and MQ-D samples, respectively. Table S4 gives 3 times the standard deviation values for the three conditions.

***Table S4**: Standard deviations for the three conditions*

Sample	MQ-D<1KD	UF-D<1KD	Raw-D<1KD	MQ
3x Std. Dev. (cps)	19340	20770	19560	16500

The detection limit of size (D_{min}) has been calculated according to [S1] and is given in Table S5.

***Table S5**: Detection limit of size, D_{min}*

Sample	MQ-D<1KD	UF-D<1KD	Raw-D<1KD	MQ
D_{min} (nm)	4	4	4	4

With the data of each sample doped with 10 nm gold NPs and their corresponding ultrafiltrated sample, using our data treatment, we can determine the size of the gold NPs and compare it to the certified value: all values are given in Table S6.

***Table S6**: Determined average size for the three matrices compared to the reference value.*

Sample	MQ-D	UF-D	Raw-D	Certified
D (nm)	10 ± 2	9 ± 2	9 ± 2	10 ± 1

The calculated size for the 10 nm certified gold nanoparticles is thus in perfect agreement with the certified value. We therefore believe that this is a strong demonstration that the calculation method for the particles number, nanoparticles mass and size for the present paper is solid and valid.

The smallest size we can detect for gold is 4 nm. A test with 10 nm TiO_2 particle was not possible since such certified material does not exist. However, our data in the present manuscript allowed to calculate a size limit of 20 ± 2 nm.

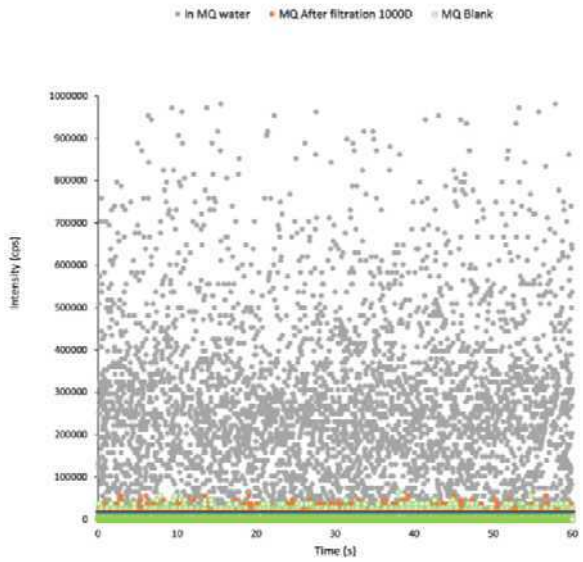

***Figure S2**: MQ solution doped with 10 nm gold NPs (gray dots), sample after ultrafiltration at 1kD (orange dots) and MQ signal (green dots). Red and blue lines correspond to three times the standard deviation of the orange and green data, respectively.*

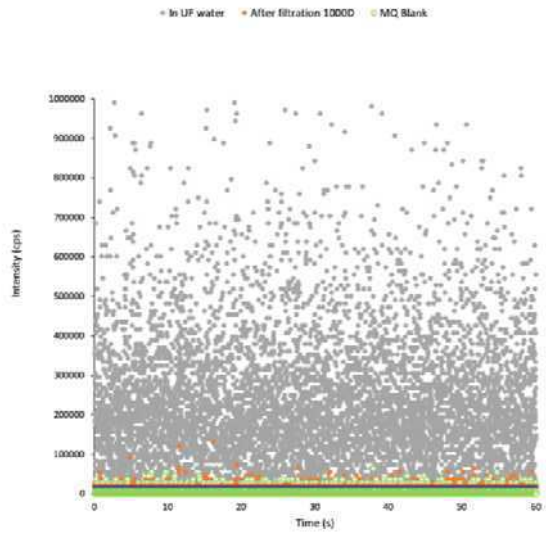

Figure S3*: Forested sample (19/12/2017) ultra-filtered solution doped with 10 nm gold NPs (gray dots), sample after ultrafiltration (1kD) (orange dots) and MQ signal (green dots). Red and blue lines corresponding to three times the standard deviation of the orange and green data, respectively.*

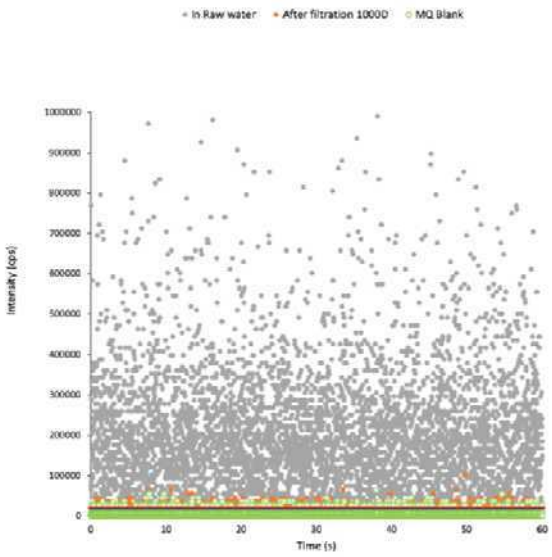

Figure S4*: Forested raw sample (19/12/2017) solution doped with 10 nm gold NPs (gray dots), sample after ultrafiltration (1kD) (orange dots) and MQ signal (green dots). Red and blue lines corresponding to three times the standard deviation of the orange and green data, respectively.*

2.3 Limit of detection of size of TiO_2 NPs by sp-ICPMS

The TiO2-NPs detection limit of size in blank from calibration curves (D_{min}) has been calculated according to the reported equation [S1]:

$$D_{\min} = \left(\frac{6 \times 3\sigma}{R \times f_a \times \rho \times \pi} \right)^{1/3} \quad (2)$$

where σ (cps) is the standard deviation of the matrix blank, R (cps μl^{-1}) is the sensitivity of the instrument for the element of the analyte, f_a is the mass fraction of the analysed metallic element in the NP and ρ is the density of the NP. In the case of TiO_2-NPs, f_a = 0.6, ρ = 4.23 g cm^3. R is the ratio of the slope of calibration curve of ionic standards solution (K at cps μl^{-1}) to η. Assuming TiO_2NPs of spherical geometry, D_{min} is equal to 20 nm in agreement with [S2].

2.4 Limit of quantification of Ti concentration by sp-ICPMS

The LOQ (C_{min}) can be calculated from the D_{min} calculated for MQ water used for the calibration and according to the following equation:

$$C_{\min} = \frac{\rho \times \pi \times \left(D_{\min} \right)^3}{6 \times q_{liq} \times t_d} \quad (3)$$

The value of $D_{min\text{-}MQ}$ equal to 20 nm gives a C_{min} of 7 ng L^{-1}, which is applied as the LOQ of Ti concentration by sp-ICPMS.

3. Evaluation of the uncertainty on nanoparticles' number concentration

According to the Guide to the expression of Uncertainty in Measurement (GUM), the standard uncertainty of measurand can be obtained by propagating the variances of the related parameters [41]. Several factors are identified as contributors to the uncertainty in case of sp-ICPMS measurements of nanoparticles in natural waters such as the solution preparation, calibration, sensitivity of ICPMS, field sampling and sample stability. Two main contributions are taken into account in this paper i.e., the measurement repeatability (u1) and the sampling variability effect (u2), for the concentration of nanoparticles determined by sp-ICPMS. The expanded uncertainty (U) was obtained for three individual sampling matrices, based on Eq. (4) and (5):

$$u = \sqrt{u_1^2 + u_2^2} \quad (4)$$

$$U = k * u \qquad (k=2) \quad (5)$$

Where u is the standard uncertainty and k is the coverage factor, chosen equal to 2, defining a level of confidence of approximately 95%. The standard uncertainty of the repeatability (u_1) was calculated using the standard deviation from 3 measurements. To evaluate the standard uncertainty of the sampling effect (u_2), six sampling replicates (F1-F6) were taken the 23/05/17, 12/07/17 and 25/09/17 in the forested, agricultural and urban catchments, respectively. Each sampling replicate is considered as one individual sample and independently analysed by sp-ICPMS with three measurements (n=3). The six sampling replicates were quantified in two separate sequences and each sequence lasted about 10 hours. Thus, u_2 provides an evaluation of the sequence's effect on the NPs concentrations in addition to the sampling variability.

To evaluate the standard uncertainty of the sampling effect (u_2), the analysis of variance (ANOVA) is applied. ANOVA is a statistical technique applied for comparing datasets, routinely used when more than two populations are involved. In this study, single-factor ANOVA, meaning comparing groups (>3) based on independent factor variable, was applied to evaluate the sampling effect. The application of the ANOVA test to quantify an effect requires that the concerned data has a normal distribution. For each type of water, 6

independent samples and 3 measurements for each sample resulted in 18 data in total. The Shapiro-Wilk test is used here to confirm normality of the 18 data.

The single-factor ANOVA test is performed with the significance level at $\alpha = 0.05$ for all data analysis. One example is given in Fig. S5, with 18 values of F1-F6 and the resume of single-factor ANOVA analysis. When $F < F_{crit}$, the sampling effect is not significant. Whereas, if $F > F_{crit}$, the sampling effect needs to be taken into account for uncertainty evaluation. In this case, the uncertainty associated with this effect can be calculated with the equation given in Fig. S5. It can be expressed as absolute number (particles mL^{-1}) or in relative uncertainty (%).

	F1	F2	F3	F4	F5	F6
NPs-TiO₂ **(particles mL⁻¹)**	73 10^6	81 10^6	84 10^6	63 10^6	84 10^6	64 10^6
	70 10^6	80 10^6	77 10^6	53 10^6	62 10^6	62 10^6
	76 10^6	75 10^6	84 10^6	67 10^6	72 10^6	72 10^6

Anova: Single Factor

Source of Variation	*SS*	*df*	*MS*	***F***	*P-value*	***Fcrit***
Between Groups	8.98 10^{14}	5	1.80 10^{14}	**4.390**	0.017	**3.106**
Within Groups	4.91 10^{14}	12	4.09 10^{13}			
Total	1.39 10^{15}	17				

u_2 68 10^6 Particles mL^{-1}
9.4 %

$$u_2 = \sqrt{\frac{MS_{between}^2 - MS_{within}^2}{n}} \quad (n=3)$$

Figure S5*: Example of single-factor ANOVA test for NPs-TiO_2 in forested water sampled on the 23th March 2017.*

Others supplementary information

Sampling date	Ti total (µg L^{-1})			Ti < 1 kDa (ng L^{-1})		
	Forested	**Agricultural**	**Urban**	**Forested**	**Agricultural**	**Urban**
30/11/2016	2	4	34	24	86	93
20/01/2017	4	21	32	29	29	87
27/02/2017	14	33	14	28	62	38
23/03/2017	16	66	10	21	31	83
23/05/2017	13	175	12	26	55	44
12/07/2017	6	182	16	11	14	15
25/09/2017	3	30	36	21	21	53
24/10/2017	7	18	26	20	25	65
21/11/2017	8	5	22	86	35	42
19/12/2017	19	24		86	35	42
Average	**9**	**56**	**22**	**35**	**39**	**56**

Table S7*: Concentration of total Ti after digestion and dissolved Ti in three watersheds throughout the year.*

	total rain month before sampling	Total rain 1 week before	average Humidity for the month	average Humidity for the week	Humidity day of sampling	Pressure month	Pressure week	Pressur day of sampling	% cloud month	%cloud week	%cloud day of sampling	Sun hour for the month	Sun hour for the week	Sun hours day sampling
TiO2 (part./mL) Forested	-0.09	-0.58	0.05	0.12	-0.01	0.08	0.27	-0.55	0.50	0.62	0.66	-0.45	-0.40	-0.63
TiO2 (part./mL) Agri.	0.70	-0.31	0.48	0.51	0.53	-0.11	0.16	-0.27	0.04	0.06	-0.23	0.37	0.34	0.51
TiO2 (part./mL) Urban	0.31	0.11	0.14	0.16	0.12	0.04	0.43	0.15	0.18	0.17	0.25	0.04	0.00	0.15

***Table S8**: Correlation matrix of average monthly nanoparticle number (n= 10) for each watershed and meteorological variables taken from https://www.historique-meteo.net/france/ile-de-france.*

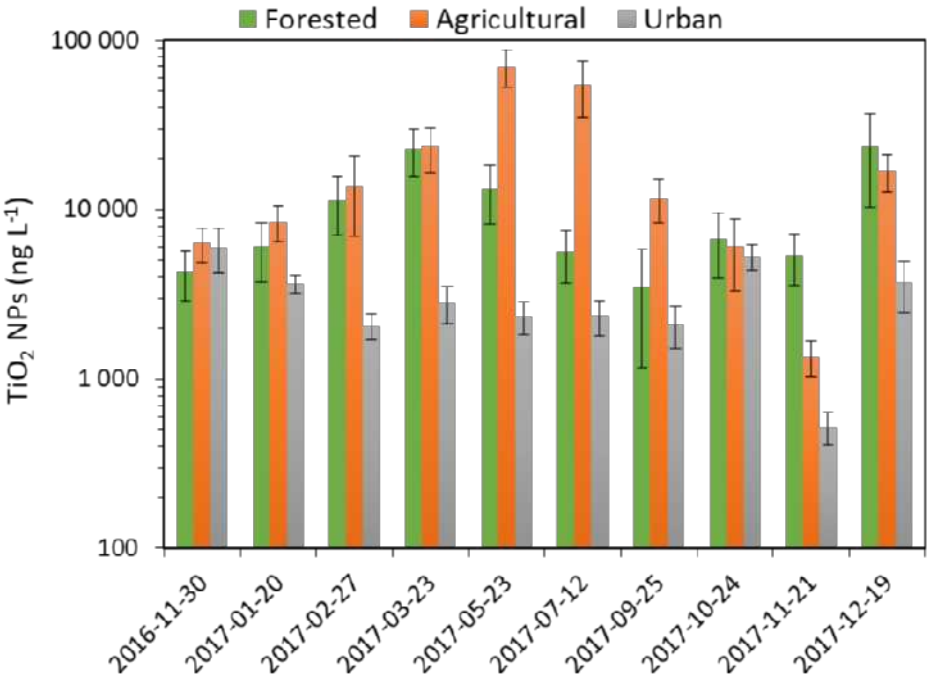

***Figure S6**: Mass concentration of TiO_2 NPs measured in water samples from three watersheds for one-year sampling.*

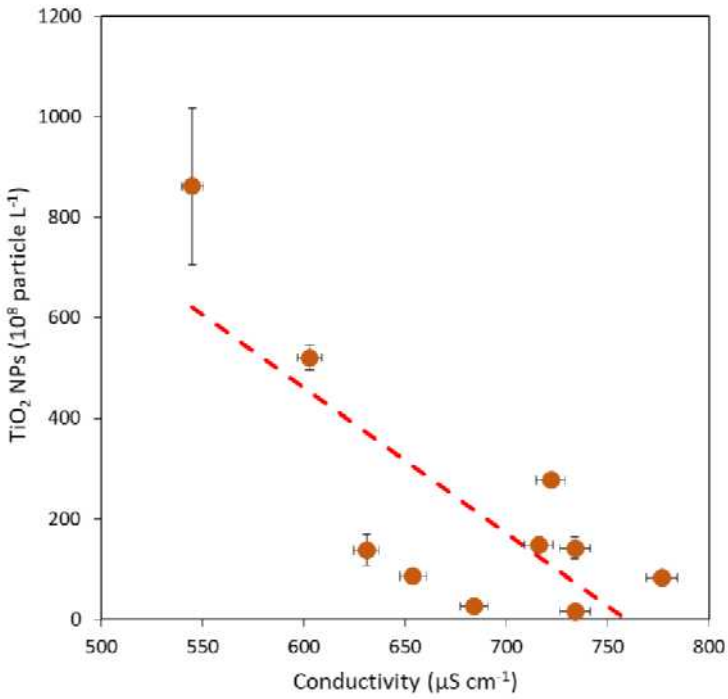

***Figure S7**: Particle number concentration of TiO2 NPs as function as conductivity in water samples from the agricultural watershed. The correlation coefficient r corresponding to the orange broken line is equal to 0.77 for a sampling size n=10.*

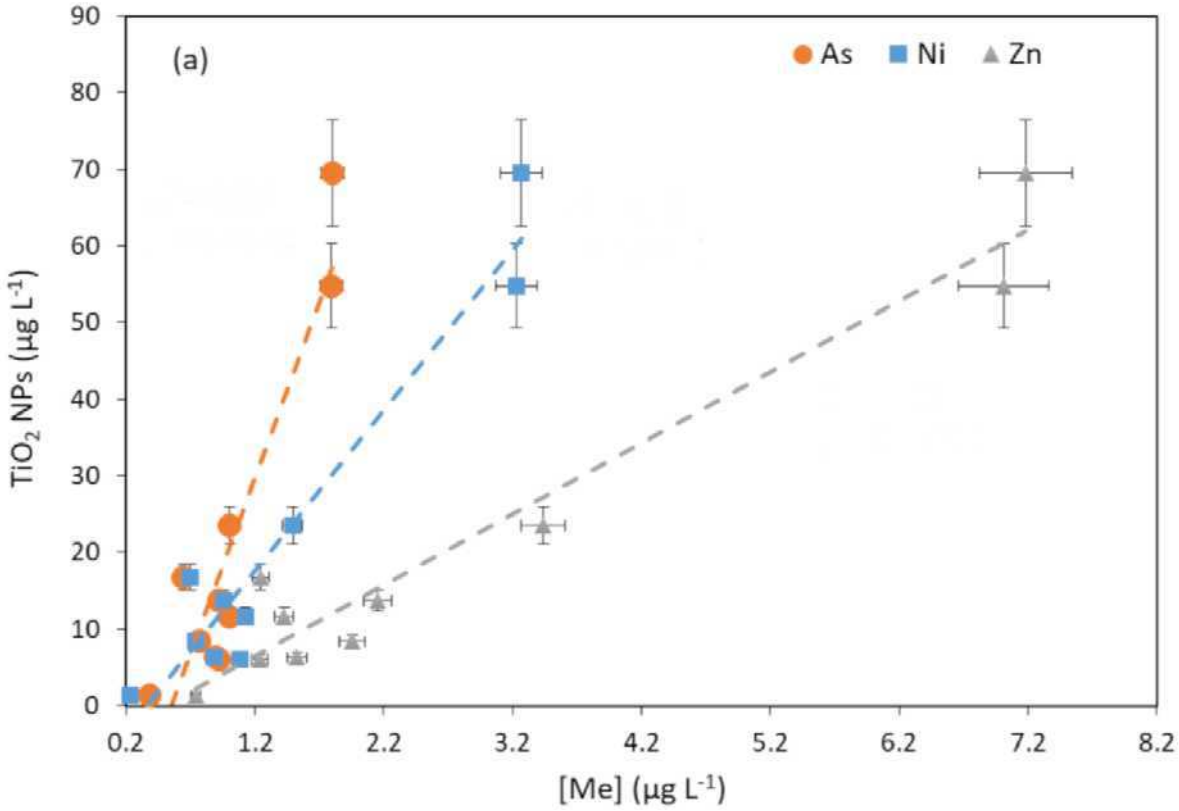

***Figure S8**: Mass concentration of TiO2 NPs as a function of that (bulk minus dissolved) of trace elements (Me) As, Ni, Zn, in agricultural water. The correlation coefficients r corresponding to As orange, Ni blue and Zn grey broken lines are equal to r_{As} = 0.92, r_{Ni} = 0.96 and r_{Zn} = 0.97. They all correspond to a p value equal to 0.00001 and a sampling size n=9*

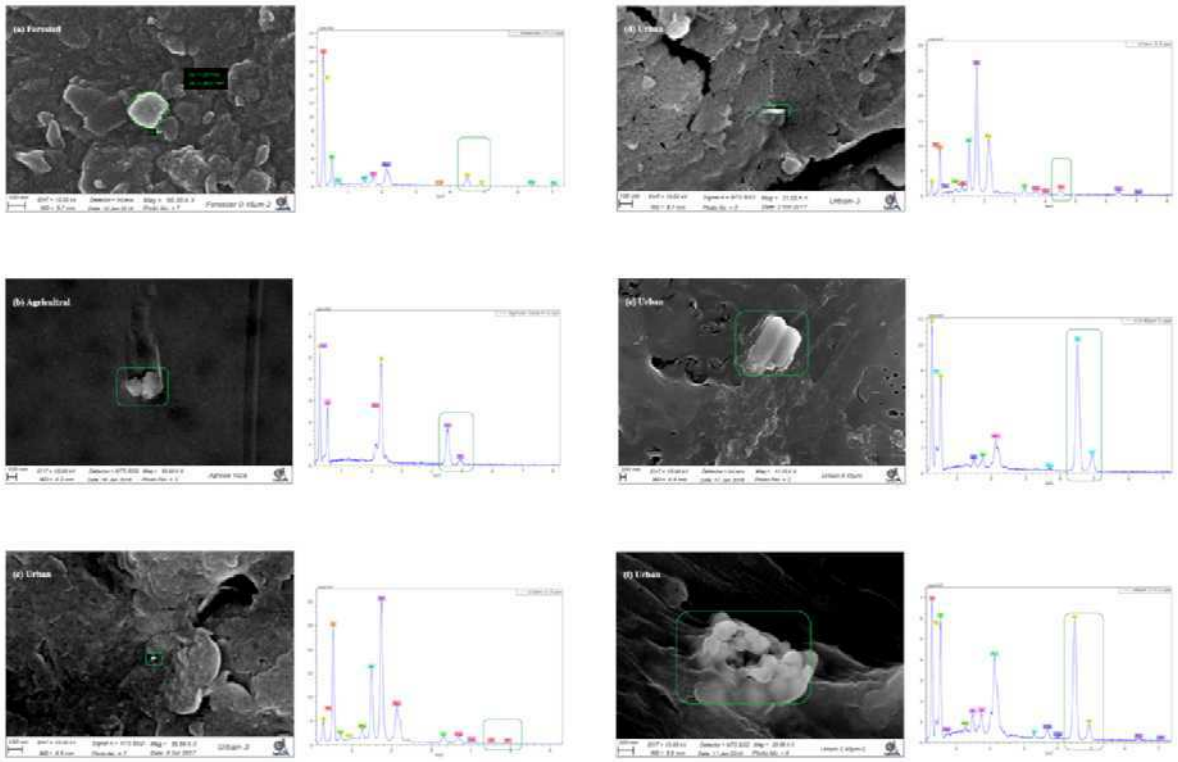

***Figure S9**: Pictures: SEM images of filters retaining suspended particles containing TiO_2 of (a, c, d) nano-scale; (e) micro-scale; (b) small aggregates; (f) large aggregates, with different shapes present in sampled waters. Graphics: showing the EDX analysis of corresponding particles highlighted by the green circle or square, showing their elemental composition.*

References

[S1] Lee, W.-W., Chan, W.-T., Calibration of single-particle inductively coupled plasma-mass spectrometry (SP-ICP-MS). J. Anal. At. Spectrom. 2015, 30, 1245–1254.

[S2] Tharaud, M., Gondikas, A.P., Benedetti, M.F., von der Kammer, F., Hofmann, T., Cornelis, G., TiO_2 nanomaterial detection in calcium rich matrices by spICPMS. A matter of resolution and treatment. J. Anal. At. Spectrom. 2017, 32, 1400–1411. https://doi.org/10.1039/C7JA00060J